Heliyon 10 (2024) e35098

Contents lists available at ScienceDirect

Heliyon

journal homepage: www.cell.com/heliyon

Review article

Strategies for improving photocatalytic performance of g-C_3N_4 by modulating charge separation and current research status

Shuangying Chen [a], Xuliang Zhang [a,b,*], Degang Li [a], Xiaowen Wang [a], Bingjie Hu [a], Fushui Guo [a], Liantao Hao [a], Bo Liu [b,**]

[a] Analysis and Testing Center, Shandong University of Technology, 266 Xincun Xi road, Zibo, 255000, PR China
[b] Laboratory of Functional Molecules and Materials, School of Physics and Optoelectronic Engineering, Shandong University of Technology, 266 Xincun Xi road, Zibo, 255000, PR China

ARTICLE INFO

Keywords:
Carbon nitride
Charge separation
Photocatalysis
Surface modification
Heterojunction

ABSTRACT

Graphitic carbon nitride (g-C_3N_4) has been extensively investigated over the past decade for its potential utilizations in photocatalytic energy generation and pollutant degradation. To better meeting the requirements for practical utilizations, it is crucial to address the issue of poor charge separation properties in g-C_3N_4, which origin from the strong interactions in photogenerated electron-hole pairs. In this review, we summarized the pertinent studies on developing strategies to promote the charge separation properties of g-C_3N_4. The strategies can be categorized into two categories of promoting the surface migration of charge carriers and prolonging the lifetime of surface charge. Finally, we present potential challenges in promoting charge separation and offer feasible suggestions to face these challenges.

1. Introduction

The burgeoning industrial and agricultural technologies has brought on a continuous exhaustion traditional fossil fuel energy resource, along with series of enormous pollution problems, such as air and water contaminations [1–6]. The progress of novel eco-friendly renewable energy sources is thus extremely urgent for solving these energy and environmental problems. Solar energy utilization by photocatalytic has caught much public attention as a hopeful technique for solving these problems since it was first developed by Fujishima and Honda in 1972 [7–10]. With the advantages of non-metal, visible-light absorption, 2D structure, easily preparation and etcetera, graphitic carbon nitride has shown its excellent potential in the field of photocatalysis and has become a hot material among varies of photocatalysts during recent years ever since it was first applied as a photocatalyst in 2009 by Xinchen Wang and his collaborators [11–17].

However, the photocatalytic performance of pristine g-C_3N_4 prepared by the traditional method of calcining raw materials directly, including urea, dicyandiamide, and melamine, is always at a low level and far below the requirement for practical applications. Therefore, series of works about g-C_3N_4 based modification materials have been carried out to improve its photocatalytic activities, such as element doping, surface modification and composite constructing [18–24]. In general, the photocatalytic reaction process can be divided into three parts from the perspective of basic photocatalytic mechanism: light absorption, separation of photogenerated

* Corresponding author. Analysis and Testing Center, Shandong University of Technology, 266 Xincun Xi road, Zibo, 255000, PR China.
** Corresponding author.
E-mail addresses: Zhangxl@sdut.edu.cn (X. Zhang), Liub@sdut.edu.cn (B. Liu).

https://doi.org/10.1016/j.heliyon.2024.e35098
Received 29 June 2024; Received in revised form 18 July 2024; Accepted 23 July 2024
Available online 24 July 2024

charges and catalytic reaction triggered by charge carriers, and thus the performance of photocatalytic reaction depends on their efficiencies (as shown in Fig. 1). Unfortunately, g-C_3N_4 always suffer from low photogenerated charge separation efficiency along with short charge carrier lifetime due to the interactions between photogenerated electrons and holes in polymeric semiconductor photocatalysts are much strong [25–28]. The weak charge separation property will make an enormous impact on the photocatalytic properties of g-C_3N_4. Therefore, for solving energy and environmental problems by photocatalysis technique, it is of great scientific significance and enormous application value to develop g-C_3N_4 based photocatalytic materials with good charge separation property. In this paper, we concentrate on strategies aimed at enhancing the charge separation of g-C_3N_4 for its application in photocatalysis. We categorize the relevant studies into two primary directions: promoting the surface migration of charge carriers and prolonging the lifetime of surface charge carriers, and an initial figure is provided for explaining the flow of this review article (as shown in Fig. 2). At last, we suggest some potential challenges on enhancing the charge separation property of g-C_3N_4.

2. Strategies on promoting surface migration of charge carriers

From the basic photocatalytic mechanism shown in Fig. 1 one can see that it is a valuable approach for enhancing its charge separation property by promoting more photogenerated charge carriers migrating to the surface of the catalyst and series of related research have thus been done based on this.

2.1. Reducing transmission distance of charge carriers

To decrease the distance of charge transmission from the charge generation site to the catalyst surface is obviously a promising way to promote surface migration of charge carriers because of the decreased body recombination phenomenon (as shown in Fig. 3). To decrease the thickness of g-C_3N_4 seems to be a very feasible and easy way for shorting the charge transmission distance and related works have thus been carried out [29,30].

Mao et al. [31] successfully synthesized thin-layer g-C_3N_4 through the method of first treated bulk g-C_3N_4 using oxalic acid solution followed by a sonication treatment. In this work, the charge separation property of the as prepared thin-layer g-C_3N_4 has been proved to be enhanced compared with the bulk one via photoluminescence spectrum and the charge lifetime is prolonged from 4.737 ns to 5.053 ns which is tested by time resolved photoluminescence. Furthermore, the enhanced charge separation property and better electronic efficiency are also proved by photo-current test and the electrochemical impedance spectroscopy results. In the study of Li and his co-workers [32], it is found that to introduce B and P into the raw material of g-C_3N_4 can break part of the hydrogen bonds within the layers and decrease the van der Waals interactions between the neighbor layers of g-C_3N_4. Under the above influences, the ultrathin g-C_3N_4 nanosheets is successfully synthesized. The charge separation property of the ultrathin g-C_3N_4 nanosheets is proved to be enhanced as prepared to the bulk one according to its sharply decreased photoluminescence signal and greatly enhanced photo-current intensity. Yang et al. [33] develop a hydrothermal treatment method using ammonium nitrate as the treating agent and finally get some thin nanosheets on the surface of bulk g-C_3N_4. As a result, the photoluminescence intensity of g-C_3N_4 greatly decreased and the photoluminescence lifetime prolonged after treating with ammonium nitrate comparing with the blank sample which indicates that the charge separation ability of the sample become better after the formation of thin nanosheets. This result is also supported by the electrochemical impedance spectroscopy and photo-current test.

Some studies pointed out that to introduce porous structure into g-C_3N_4 is also a feasible structure modification method for promoting its charge separation property [34,35]. For example, Yin et al. [36] prepared porous g-C_3N_4 via a self-assembly method employing sodium persulfate as the modifier. Through photoluminescence spectroscopy, electrochemical impedance spectroscopy, and transient photocurrent response, it has been demonstrated that the porous structure confers enhanced charge separation properties

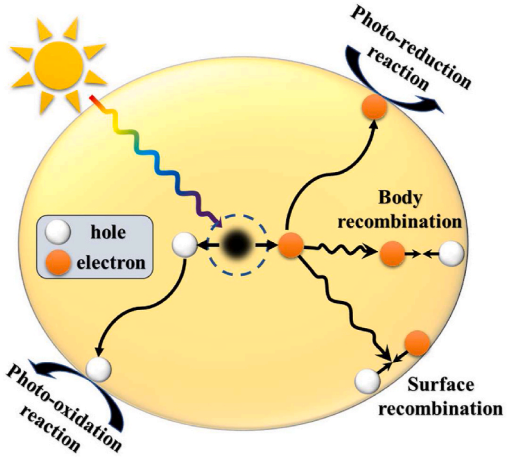

Fig. 1. Basic process of semiconductor-based photocatalytic reaction.

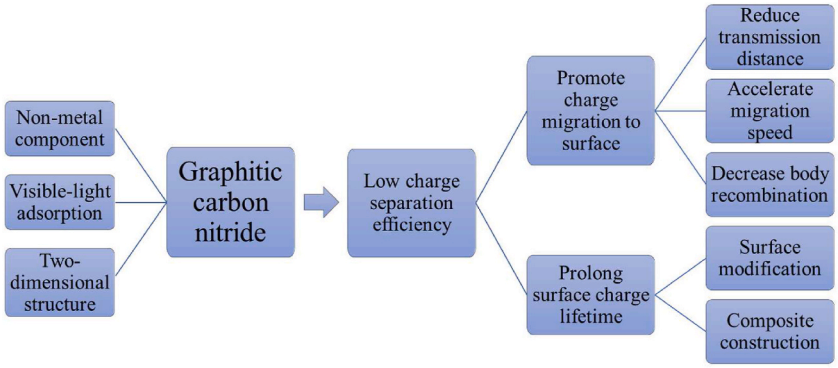

Fig. 2. Initial figure for the flow of this review article.

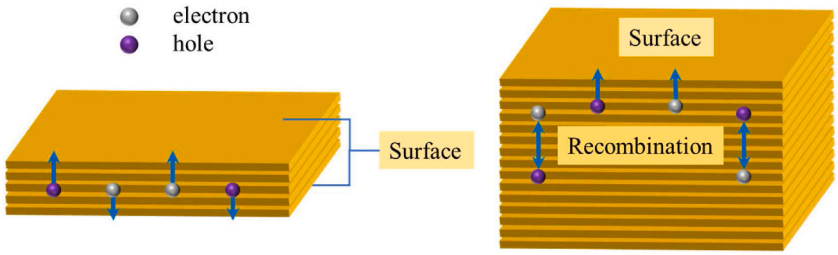

Fig. 3. Charge separation comparison between thin and thick g-C_3N_4.

to g-C_3N_4, thus improving its photocatalytic H_2 evolution performance. Liu et al. [37] successfully synthesized mesoporous g-C_3N_4 with a horn-like hollow morphology through initially forming a horn-like Br-containing intermediate, subsequently undergoing decomposition transformation via co-pyrolysis of melamine and a significant amount of NH_4Br. The final sample is proved to exhibit enhanced charge separation property along with improved H_2 evolution activity. From my point of view, as g-C_3N_4 is a natural sheet structural material and its mainly charge transmission is along the direction which perpendicular to the sheet layers [38], it is deduced that the localized thickness decrease of g-C_3N_4 is also the fundamental reason for shortening the charge transmission distance by constructing porous structure (as shown in Fig. 4).

Another strategy taken out by some studies for shorting the charge transfer distance from the photogenerated charge separation position to the surface of g-C_3N_4 is to decrease the distance between the neighboring layers (as shown in Fig. 5).

Chen and the co-workers [39] used the solution of urea and thiourea dissolved in isopropanol as precursor, then treat it with a hydrothermal process to ignite the pre-polymerization of urea and thiourea following by the polymerization process through calcination treatment. Finally, they successfully synthesized g-C_3N_4 with shortened interlayer distance. Compared with the normal interlayer distance g-C_3N_4, this g-C_3N_4 shows much weaker photoluminescence intensity, increased photoluminescence lifetime and

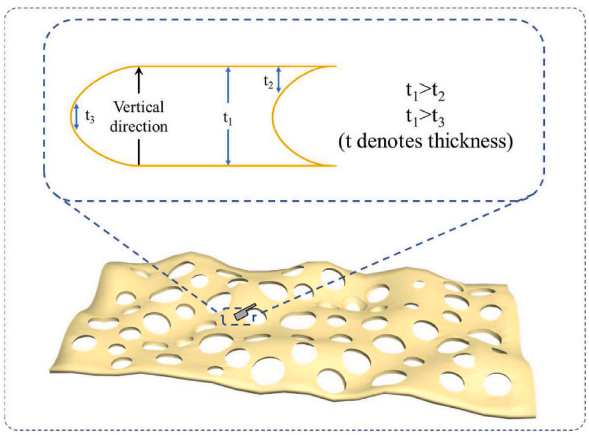

Fig. 4. The contribution mechanism of hole structure construction to decrease the thickness of g-C_3N_4.

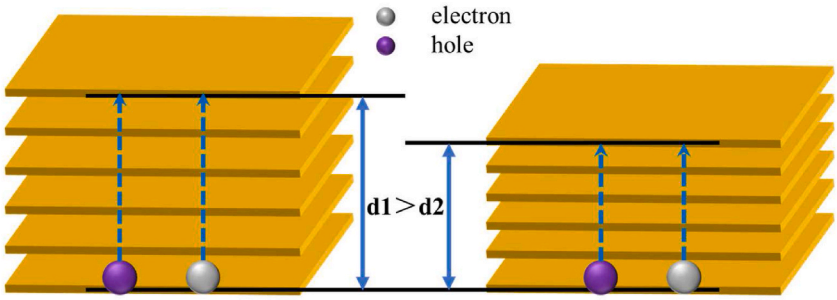

Fig. 5. Schematic diagram of shorting charge transfer distance by decreasing the distance between the neighboring layers.

smaller arc radius in electrochemical impedance spectroscopy, which can prove the enhanced charge separation property of the interlayer distance shortened g-C_3N_4 from the point of physics. Further measurements of photo-current test based on the photochemical experiment, superoxide radical test and hydroxyl radical test based on the electron spin resonance measurement are also carried out for better support the charge separation enhancement from the point of chemistry. The interlayer distance shortened g-C_3N_4 is proved to have better charge separation property based on these results. Shi and the co-workers [40] prepared a nitrogen deficient g-C_3N_4 by using tartaric acid and dicyandiamide as precursors, and proved that the layer stacking distance is decreased by this method which is beneficial to the mobility of charge carriers to surface of the material. Besides, by doping potassium into the framework can also decrease the interlayer distance of g-C_3N_4, which is reported in the work of Kang et al. [41].

2.2. Accelerating migration speed of charge carriers

Even though decreasing the distance of charge migration is an effective strategy for promoting photogenerated charge carriers transfer to the surface of the g-C_3N_4, it is suggested that to accelerate the charge carrier migration speed will make it more sufficient and related strategies about promoting the charge migration have thus been developed. To provide some charge transmission channels which are valuable for the photogenerated charges to go through (as shown in Fig. 6) is supposed to be an effective strategy for accelerating the charge migration speed [42–45].

Xiong et al. [42] prepared K-doped g-C_3N_4 via a method of directly calcinating the pre-mixed precursor. By means of many measurements, including DFT calculations, XRD test, XPS technique, photoelectrochemical test, steady-state photoluminance and transient-state photoluminance, it is demonstrated that the doped K will be inserted into the g-C_3N_4 interlayer and thus linking the layers, which is favorable to the photogenerated charge transfer between adjacent layers. In their subsequent study [44], the K and Cl co-doped g-C_3N_4 was further prepared via the same method, and the K and Cl is proved to be the transmission channel for electrons and holes, respectively. The resultant sample exhibits enhanced charge separation property and better photocatalytic performance for NO_x removal as compared to both the pristine g-C_3N_4 and K-doped g-C_3N_4. Li and the co-workers [43] synthesized Rb-doped g-C_3N_4 and Cs-doped g-C_3N_4, which exhibits enhanced NO removal performance and promoted charge separation property as compared to the pristine one, through a facile co-pyrolysis method. The Rb and Cs. By means of DFT calculation, in-situ ESR spectroscopy and transient-state photoluminance, the mechanism for the enhanced charge separation property is investigated. The doped Rb and Cs atoms in the g-C_3N_4 interlayers provide vertical channels and promote electron migration, leading to better charge separation property.

2.3. Decreasing body recombination of charge carriers

To promote the migration of charge carriers to the surface of g-C_3N_4, it is imperative to address the body recombination of electron-

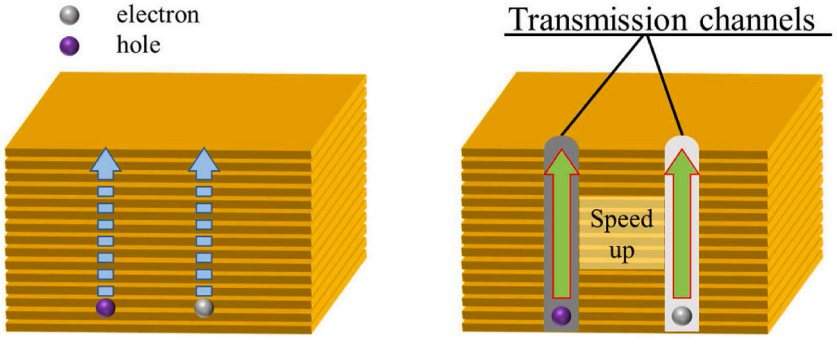

Fig. 6. Mechanism schematic of charge transmission channels providing strategy.

hole pairs. Suppression of the bulk charge carriers recombination will result in a prolonged lifetime for photo-induced electrons and holes, thereby increasing their opportunity of diffusion to the material surface (as shown in Fig. 7). Investigations aimed at suppressing the bulk charge recombination have thus been studied to facilitate photogenerated electron-hole pairs migrating from the bulk of the catalyst to its surface.

Bellamkonda et al. [46] also introduced benzene rings into the molecular skeleton of g-C_3N_4 by copolymerizing melamine and 1,3, 5-triaminobenzene. Through the DFT calculations, photoluminescence spectra, electron paramagnetic resonance spectra, photocurrent measurement and electrochemical impedance spectra results, it is demonstrated that the charge separation property of g-C_3N_4 is enhanced by introducing benzene rings, and its mechanism is suggested that the charge densities over the valence band maxima and conduction band minima were localized in different parts of heptazine rings, resulting in the reduced recombination rate of charge carriers. Liang and the co-workers [47] prepared tin-doped g-C_3N_4 through the calcination of a precursor derived from the evaporation of a homogeneously pre-mixed solution containing urea and $(NH_4)_2SnCl_6$. By mean of photoluminescence spectra, time-resolved fluorescence spectra, photocurrent density, electrochemical impedance spectra and DFT calculation of the samples, it is indicated that the photogenerated holes tend to migrate to the N–Sn bonds and separated with the photogenerated electrons, the recombination of charge carrier is thus suppressed and the holes on N–Sn bond will participate in the oxidation reaction, while the electrons will participate in the production of H_2. Yang et al. [48] engineered structural defects within g-C_3N_4 by substituting a portion of the nitrogen atoms at the edges of the heptazine units with oxygen atoms and by introducing cyano group into the g-C_3N_4 plane. Through various of measurements, such as photoluminescence emission spectra, time-resolved photoluminescence decay spectra, electron paramagnetic resonance spectra, electrochemical impedance spectroscopy and photoelectrochemical performances, it is suggested that the introduced structural defects act as traps for photogenerated electrons, redistributing these electrons within the melon units. This facilitates the migration and transference of electrons across the plane, consequently leading to a suppressed charge carrier recombination. Liang et al. [49] successfully synthesized Sb-doped g-C_3N_4 by employing a calcination process on the pre-mixed precursors utilizing $NaSbO_3$ and urea as the raw materials. By means of DFT calculations and related experimental analyses, it has been confirmed that the Sb doping results in the formation of N–Sb bonds, subsequently introducing two impurity energy levels, designated as E_N and E_S, which function as a hole-capture center and an electron-capture center respectively, this doping of Sb thus significantly enhances the charge separation properties of g-C_3N_4.

Several related works about promoting charge separation property of g-C_3N_4 by the above-mentioned strategies have been summarized in Table 1.

3. Strategies on prolonging lifetime of surface charge carriers

Based on the above description, varies of strategies developed can promote charge carriers migrating to the surface of the catalyst effectively. However, the problem of quickly recombination between photo-induced electrons and holes on the surface of the catalyst is seriously influencing the lifetime of surface charge carriers. As the chemical reaction usually happens at the timescale of microsecond while the recombination of photoexcited electron-hole pairs occurs at a faster timescale, it is important to prolong the lifetime of surface charge carriers for enhancing the charge separation property of g-C_3N_4, and spatial separation of electron-hole pairs to decrease their recombination possibility is thus necessary. According to the above description, developing strategies to promote the spatial separation of surface photoexcited electron-hole pairs for prolonging their lifetime is essential for enhancing the charge separation property of g-C_3N_4.

3.1. Surface modification

From the perspective of semiconductor physics, it is proposed that achieving charge transfer through the modification of certain functional groups with the ability of accepting photoexcited electrons or holes on the surface of photocatalysts constitutes a feasible strategy for prolonging the lifetime of photogenerated charges as this transference can facilitate the spatial separation of electrons and holes (as shown in Fig. 8). Consequently, related studies have been conducted based on this strategy.

Some studies focusing on modulating the photogenerated electrons have been carried out. Wang et al. [62] successfully synthesized carbon-modified g-C_3N_4 through a facile one-step pyrolysis process, which involved the direct thermal treatment of a blended mixture of melamine and soybean oil. Based on the electrochemical impedance spectroscopy and photoluminescence spectroscopy results, it

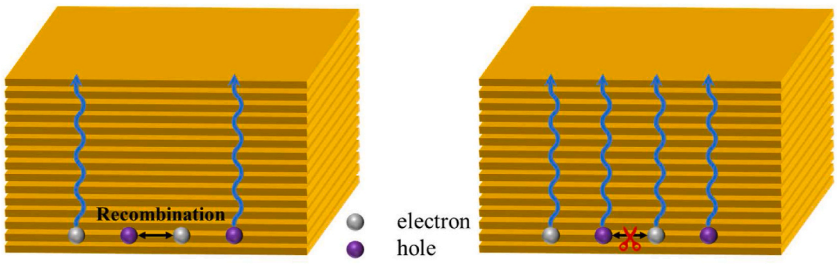

Fig. 7. Mechanism schematic of promoting charge separation by suppressing the bulk recombination of photogenerated electron-hole pairs.

Table 1
Works on promoting surface migration of charge carriers.

strategy	Method	Application	Reaction situation	Performance	Ref.
Reducing transmission distance of charge carriers	Dop B and P	H_2 evolution	Arc lamp ($\lambda \geq 400$ nm), triethanolamine as sacrificial agent, Pt as co-catalyst.	10877.4 μmol h^{-1} g^{-1}	[32]
Same as above	NH_4HCO_3 as template	H_2 evolution, RhB degradation	H_2 evolution: 300 W Xe lamp ($\lambda \geq 420$ nm), lactic acid as sacrificial agent, Pt as co-catalyst. RhB degradation: 500 W Xe lamp ($\lambda \geq 420$ nm), 0.02 mM of RhB, 1 mg mL^{-1} of photocatalyst.	H_2 evolution: 1216 μmol h^{-1} g^{-1} RhB degradation: 0.92 h^{-1}	[34]
Same as above	NH_4NO_3-assisted hydrothermal treatment	H_2 evolution	300 W Xe lamp ($\lambda \geq 420$ nm), triethanolamine as sacrificial agent, Pt as co-catalyst.	11817.9 μmol h^{-1} g^{-1}	[33]
Same as above	Hydrothermal and thermal etching treatments	Disinfection of *Escherichia coli*, methylene blue degradation	Disinfection: 500 W Xe lamp ($\lambda \geq 420$ nm), 5×106 cfu mL^{-1} of *Escherichia coli*, 0.4 mg mL^{-1} of photocatalyst. Degradation: 500 W Xe lamp ($\lambda \geq 420$ nm), 1.2×10^{-5} M of methylene blue, 0.2 mg mL^{-1} of photocatalyst.	Disinfection: 100 % at 4 h Degradation: 0.551 h^{-1}	[35]
Same as above	Ultrasonic exfoliation	Aflatoxin B_1 degradation	500 W Xe lamp ($\lambda \geq 400$ nm), 0.5 μg mL^{-1} of Aflatoxin B_1, 0.1 mg mL^{-1} of photocatalyst.	70.2 % at 120 min	[31]
Same as above	Co-pyrolysis of melamine and ammonium bromide	H_2 evolution, CO_2 reduction	H_2 evolution: 300 W Xe lamp ($\lambda \geq 420$ nm), Pt as co-catalyst. CO_2 reduction: 300 W Xe lamp.	H_2 evolution: 1354 μmol h^{-1} g^{-1} CO_2 reduction: 10.8 μmol h^{-1} g^{-1} (CO)	[37]
Same as above	$Na_2S_2O_8$ regulated self-assembly of melamine	H_2 evolution	300 W Xe lamp ($\lambda \geq 420$ nm), triethanolamine as sacrificial agent, Pt as co-catalyst.	604 μmol h^{-1} g^{-1}	[36]
Same as above	KCl and LiCl modulated quench method	H_2 evolution, H_2O_2 production	H_2 evolution: 300 W Xe lamp ($\lambda \geq 420$ nm), triethanolamine as sacrificial agent, Pt as co-catalyst. H_2O_2 production: 300 W Xe lamp ($\lambda \geq 420$ nm), isopropanol as sacrificial agent.	H_2 evolution: 10600 μmol h^{-1} g^{-1} H_2O_2 production: 6600 h^{-1} g^{-1}	[30]
Same as above	HCl and NH_4Br modulation	H_2 evolution, RhB degradation	H_2 evolution: 300 W Xe lamp ($\lambda \geq 420$ nm), triethanolamine as sacrificial agent, Pt as co-catalyst. RhB degradation: 500 W Xe lamp ($\lambda \geq 420$ nm), 10 mg L^{-1} of RhB, 0.4 mg mL^{-1} of photocatalyst.	H_2 evolution: 1412 μmol h^{-1} g^{-1} RhB degradation: 1.34 h^{-1}	[50]
Same as above	Recalcination treatment and Hexamethylenetetramine-assisted tertiary calcination	H_2 evolution	300 W Xe lamp, triethanolamine as sacrificial agent, Pt as co-catalyst.	27035.23 μmol h^{-1} g^{-1}	[29]
Same as above	Tartaric acid assistant thermal polymerization of dicyandiamide	CO_2 reduction	300 W Xe lamp ($\lambda \geq 400$ nm), methyl cyanide solution contains triethanolamine, bipyridine and $CoCl_2$.	56.94 μmol h^{-1} g^{-1} (CO)	[40]
Same as above	isopropanol assisted solvothermal-copolymerization	H_2 evolution, RhB degradation	H_2 evolution: 300 W Xe lamp ($\lambda \geq 420$ nm), triethanolamine as sacrificial agent, Pt as co-catalyst. RhB degradation: 500 W Xe lamp ($\lambda \geq 420$ nm), 10 mg L^{-1} of RhB, 0.5 mg mL^{-1} of photocatalyst.	H_2 evolution: 3643.3 μmol h^{-1} g^{-1} RhB degradation: 7.2 h^{-1}	[39]
Same as above	Treatments of molecular assemble, alcohol molecules intercalation, thermal-induced exfoliation and polycondensation	H_2 evolution	300 W Xe lamp, triethanolamine as sacrificial agent, Pt as co-catalyst.	7990 μmol h^{-1} g^{-1}	[51]
Accelerating migration speed of charge carriers	Dop K	NO removal	Air flow rate: 2.4 L min^{-1}, NO (100 ppm) flow rate: 15 mL min^{-1}, 150 W tungsten halogen lamp ($\lambda \geq 420$ nm), 0.2 g of sample.	36.8 %	[42]
Same as above	Dop Cs	NO removal	Air flow rate: 2.4 L min^{-1}, NO (100 ppm) flow rate: 15 mL	48.23 %	[43]

(*continued on next page*)

Table 1 (*continued*)

strategy	Method	Application	Reaction situation	Performance	Ref.
			min^{-1}, 150 W tungsten halogen lamp ($\lambda \geq 420$ nm), 0.2 g of sample.		
Same as above	Dop KCl	NO removal	Air flow rate: 2.4 L min^{-1}, NO (100 ppm) flow rate: 15 mL min^{-1}, 150 W tungsten halogen lamp ($\lambda \geq 420$ nm), 0.2 g of sample.	38.4 %	[44]
Same as above	Intercalate atomic Pd into the adjacent layers	H_2 evolution	300 W Xe lamp.	≈6500 μmol h^{-1} g^{-1}	[52]
Same as above	Intercalation of K^+ and NO_3^- species	NO oxidation	150 W tungsten halogen lamp, 0.2 g of sample, 500 ppb continuous flow.	41.93 %	[45]
Decreasing body recombination of charge carriers	Dop Mn	CO_2 reduction	300 W Xe lamp, water as sacrificial agent.	47 μmol h^{-1} g^{-1} (CO)	[53]
Same as above	Implant carbon quantum dot	H_2 evolution	300 W Xe lamp ($\lambda \geq 400$ nm), methanol as sacrificial agent, Pt as co-catalyst.	3538.3 μmol h^{-1} g^{-1}	[54]
Same as above	Dop benzene molecule	H_2O_2 production	300 W Xe lamp ($\lambda \geq 420$ nm), ethanol as sacrificial agent, 0.5 g L-1 of photocatalyst.	≈300 μM at 3 h	[55]
Same as above	Dop phosphorus	H_2 evolution	300 W Xe lamp ($\lambda \geq 420$ nm), triethanolamine as sacrificial agent, Pt as co-catalyst.	2610.80 μmol h^{-1} g^{-1}	[56]
Same as above	Dop manganese	RhB degradation, MO degradation	500 W Xe lamp ($\lambda \geq 420$ nm), 10 mg L^{-1} of pollutant, 0.4 mg mL^{-1} of photocatalyst.	RhB degradation: 3.46 h^{-1} MO degradation: 0.0417 h^{-1}	[57]
Same as above	Dop benzene	H_2 evolution	300 W Xe lamp ($\lambda \geq 450$ nm), Pt as co-catalyst.	140 μmol h^{-1} g^{-1}	[46]
Same as above	Dop tin	H_2 evolution	300 W Xe lamp ($\lambda \geq 420$ nm), triethanolamine as sacrificial agent, Pt as co-catalyst.	1690 μmol h^{-1} g^{-1}	[47]
Same as above	Ascorbic acid assisted method to introducing oxygen element and cyano group into g-C_3N_4 nanosheets	H_2 evolution	300 W Xe lamp ($\lambda \geq 420$ nm), triethanolamine as sacrificial agent, Pt as co-catalyst.	1336.8 μmol h^{-1} g^{-1}	[48]
Same as above	In-plane implant carbon rings	Naproxen degradation	500 W Xe lamp ($\lambda \geq 420$ nm), 20 mg L^{-1} of naproxen, 60 mg L^{-1} of photocatalyst.	100 % in 1 h	[58]
Same as above	Graft 2-hydroxy-4,6-dimethylpyrimidine	Oxytetracycline degradation, H_2O_2 production	Oxytetracycline degradation: 300 W Xe lamp ($\lambda \geq 420$ nm), 20 mg L^{-1} of oxytetracycline, 0.3 mg mL^{-1} of photocatalyst. H_2O_2 production: 300 W Xe lamp ($\lambda \geq 420$ nm), isopropanol as sacrificial agent, 1 mg mL^{-1} of photocatalyst.	Oxytetracycline degradation: 1.74 h^{-1} H_2O_2 production: 174 μmol h^{-1} g^{-1}	[59]
Same as above	Dop basic fuchsin	H_2 evolution	300 W Xe lamp ($\lambda \geq 420$ nm), triethanolamine as sacrificial agent, Pt as co-catalyst.	1619 μmol h^{-1} g^{-1}	[60]
Same as above	Dop benzene	H_2 evolution	300 W Xe lamp ($\lambda \geq 420$ nm), triethanolamine as sacrificial agent, Pt as co-catalyst.	12543 μmol h^{-1} g^{-1}	[61]
Same as above	Dop Sb	H_2 evolution	300 W Xe lamp ($\lambda \geq 420$ nm), triethanolamine as sacrificial agent, Pt as co-catalyst.	1750 μmol h^{-1} g^{-1}	[49]

has been confirmed that the photogenerated electrons in g-C_3N_4 are transferred to the modified carbon, thereby facilitating an efficient separation from the photogenerated holes, which consequently leads to a significantly enhanced photogenerated charge separation efficiency. Wang et al. [63] prepared single Ni atom decorated g-C_3N_4 via a boric-acid mediated method. By means of steady-state photoluminescence, hydroxyl radical test, transient absorption spectra, transient-state surface photovoltage analysis, steady-state surface photovoltage spectroscopy and transient-state photoluminescence analysis, it has been demonstrated that the single Ni sites which anchored on the g-C_3N_4 surface will effectively capturing the photoelectrons, leading to a facilitated charge separation property and prolonged charge lifetime. Xue et al. [64] successfully synthesized a molecularly engineered g-C_3N_4 by utilizing anthraquinone-2-carboxylic acid as the modifier, wherein the peptide bond is formed through the reaction between the –COOH group in anthraquinone-2-carboxylic acid and the –NH_2 group in g-C_3N_4, serving as the linking mechanism. Through DFT calculations and

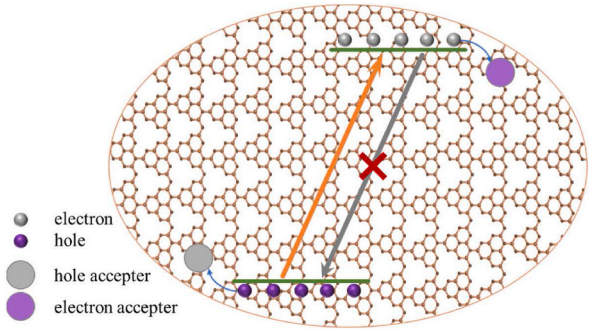

Fig. 8. Mechanism schematic of accelerating charge separation by accepting photoexcited electrons or holes.

related experimental analyses, including photoluminescence spectroscopy, time-resolved fluorescence spectra, electron paramagnetic resonance analysis, electrochemical impedance spectroscopy and electrochemical measurements, it has been demonstrated that the modified molecule works as an electron acceptor, thereby enhancing the efficiency of electron-hole separation and prolonging the lifetime of charge carriers.

Some studies focusing on modulating the photogenerated holes have been reported. Liu et al. [65] successfully modified 1, 1′-ferrocene dicarboxylic acid on the surface of g-C_3N_4 utilizing a facile sonication attaching and anchoring method. Based on photoluminescence spectroscopy, time-resolved fluorescence response, transient photocurrent response and electrochemical impedance spectroscopy, it has been demonstrated that the photogenerated holes can be effectively transferred from g-C_3N_4 to the modified 1, 1′-ferrocene dicarboxylic acid groups, thereby suppressing the recombination of charge carriers and prolong the charge lifetime. Cl-modified g-C_3N_4 was successfully synthesized by Li et al. using a wet-chemical method [66]. Various characterization techniques, including steady-state surface photovoltage spectroscopy, atmosphere-controlled time-resolved surface photovoltage technique, photoluminescence spectroscopy, and hydroxyl radical tests, were employed to verify its charge separation properties. The results conclusively demonstrate that the introduction of Cl on the surface of g-C_3N_4 leads to effective modulation of photogenerated holes, resulting in a notable decrease in the recombination of electron-hole pairs and consequently prolonging the lifetime of the charge carriers. Zeng and the coworkers [67] achieved successful construction of a g-C_3N_4 material grafted with poly-ethylenimine molecules using a pH-modulated electrostatic attraction method. Extensive investigations using DFT calculations and various experimental techniques, such as photoelectrochemical analysis, electrochemical impedance spectroscopy, surface potential mapping analysis, and electron paramagnetic resonance test, have convincingly shown that the presence of poly-ethylenimine effectively traps the photo-induced holes, thus inhibiting charge recombination.

Efforts have also been made to explore the simultaneous modulation of photogenerated electrons and holes. Ren et al. [68] successfully fabricated Ag and BN quantum dots co-modified g-C_3N_4 through photo-reduction and wet chemical synthesis techniques. By means of photoluminescence spectroscopy, time-resolved fluorescence response, photo-current response, and electrochemical impedance spectroscopy, it has been evidenced that the strategically modified Ag and BN quantum dots on the g-C_3N_4 surface independently capture photo-induced electrons and holes, consequently prolonging the lifetime of the charge carriers. Zhang and colleagues successfully synthesized Co and Ni co-modified g-C_3N_4 utilizing a facile in-situ pre-assembly method [69]. Employing various of charge separation property analysis techniques, including photoluminescence spectroscopy, steady-state surface photovoltage spectroscopy, time-resolved fluorescence decay response, and transient-state surface photovoltage response, it has been revealed that the modified Co will accept the holes while the modified Ni will accept the electrons generated by g-C_3N_4, thereby to prolong the lifetime of the charge carriers.

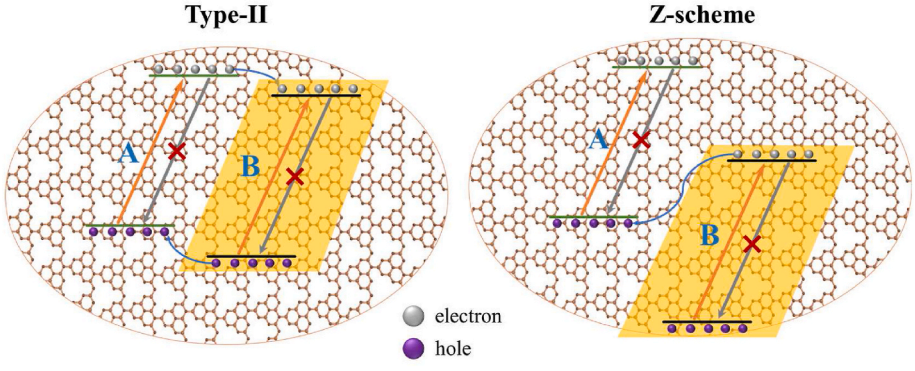

Fig. 9. Mechanism schematic of the charge transfer in type-II and Z-scheme structures.

Table 2
Works on prolonging lifetime of surface charge carriers.

strategy	Method	Application	Reaction situation	Performance	Ref.
Surface modification	Integrate the metal alloy of Pt and Au	H_2 evolution	300 W Xe lamp, Na_2SO_3 and Na_2S as sacrificial agent.	1009 μmol g^{-1} h^{-1}	[80]
Same as above	Anchor single Ni atoms	CO_2 reduction	300 W Xe lamp, water as sacrificial agent.	22.1 μmol g^{-1} h^{-1} (CO) 8.7 μmol g^{-1} h^{-1} (CH_4)	[63]
Same as above	Modify red phosphorus	H_2 evolution	300 W Xe lamp (λ ≥ 400 nm), triethanolamine as sacrificial agent, Pt as co-catalyst.	2565 μmol h^{-1} g^{-1}	[81]
Same as above	Dop potassium and modify 1,2-benzisothiazolin-3-one	H_2 evolution	300 W Xe lamp (λ ≥ 365 nm), triethanolamine as sacrificial agent, Pt as co-catalyst.	21350 μmol h^{-1} g^{-1}	[82]
Same as above	Embed carbon	H_2 evolution	300 W Xe lamp (λ ≥ 420 nm), triethanolamine as sacrificial agent, Pt as co-catalyst.	718.1 μmol h^{-1} g^{-1}	[83]
Same as above	Anchor 2,4,5-trichlorophenoxyacetic acid	H_2 evolution	300 W Xe lamp (λ ≥ 420 nm), triethanolamine as sacrificial agent, Pt as co-catalyst.	1845 μmol h^{-1} g^{-1}	[84]
Same as above	Introduce carbon	CO_2 reduction	500 W Xe lamp, H_2O as sacrificial agent.	22.6 μmol g^{-1} h^{-1} (CO) 12.59 μmol g^{-1} h^{-1} (CH_4)	[62]
Same as above	Introduce MoP	H_2 evolution	300 W Xe lamp (λ ≥ 400 nm), triethanolamine as sacrificial agent.	3868 μmol g^{-1} h^{-1}	[85]
Same as above	Modify Pd nanoparticles	H_2 evolution	300 W Xe lamp (λ ≥ 400 nm), triethanolamine as sacrificial agent.	5358 μmol g^{-1} h^{-1}	[86]
Same as above	Modify RhP_x nano-species	H_2 evolution	300 W Xe lamp (λ ≥ 420 nm), triethanolamine as sacrificial agent.	3055.9 μmol g^{-1} h^{-1}	[87]
Same as above	Implant carbon quantum dot	Tetracycline degradation, RhB degradation	Tetracycline degradation: 40 W LED lamp, 40 mL of tetracycline solution (40 mg L^{-1}), 20 mg of photocatalyst. RhB degradation: 40 W LED lamp, 40 mL of RhB solution (10 mg L^{-1}), 10 mg of photocatalyst.	Tetracycline degradation: 1.20 h^{-1} RhB degradation: 2.04 h^{-1}	[88]
Same as above	Dop carbon species and introduce N defects	Sulfamethazine degradation	300 W Xe lamp (λ ≥ 420 nm), 30 mL of RhB solution (30 mg L^{-1}), 10 mg of photocatalyst.	1.662 h^{-1}	[89]
Same as above	Introduce carbonized poly-(furfural alcohol)	H_2 evolution	300 W Xe lamp (λ ≥ 400 nm), triethanolamine as sacrificial agent, Pt as co-catalyst.	584.7 μmol g^{-1} h^{-1}	[90]
Same as above	Modify anthraquinone-2-carboxylic acid	H_2O_2 production	300 W Xe lamp (λ ≥ 420 nm), isopropanol as sacrificial agent.	36.41 mM h^{-1} g^{-1}	[64]
Same as above	in situ surface P-N bond modulation	H_2 evolution	300 W Xe lamp (λ ≥ 400 nm), triethanolamine as sacrificial agent, Pt as co-catalyst.	1800 μmol g^{-1} h^{-1}	[91]
Same as above	Introduce 1,1′-ferrocenedicarboxylic acid	H_2 evolution	300 W Xe lamp (λ ≥ 420 nm), triethanolamine as sacrificial agent, Pt as co-catalyst.	1558.2 μmol g^{-1} h^{-1}	[65]
Same as above	surface polarization by introducing halogen elements	CO_2 reduction, 2, 4-DCP degradation	CO_2 reduction: 300 W Xe lamp, H_2O as sacrificial agent. 2, 4-DCP degradation: 150 W Xe lamp, 0.15 g of photocatalyst, 60 mL of 2,4-DCP (10 mg L^{-1}).	CO_2 reduction: 14 μmol g^{-1} h^{-1} (CH_4) 2, 4-DCP degradation: ≈40 % at 1.5 h	[66]
Same as above	Incorporate *para*-phenylene	H_2 evolution	300 W Xe lamp (λ ≥ 420 nm), triethanolamine as sacrificial agent, Pt as co-catalyst.	386 μmol g^{-1} h^{-1}	[92]
Same as above	Introduce nickel complex and NiO_x	H_2 evolution	300 W Xe lamp (λ ≥ 420 nm), triethanolamine as sacrificial agent.	524.1 μmol g^{-1} h^{-1}	[93]
Same as above	Graft cationic polyethyleneimine	H_2O_2 generation,	1000 W m^{-2} with AM 1.5 air filter.	208.1 μmol g^{-1} h^{-1}	[67]
Same as above	Introduce BN quantum dots and Ag nanoparticles	Tetracyclines degradation, Cr (VI) reduction	Tetracyclines degradation: 300 W Xe lamp (λ ≥ 420 nm), 50 mg of sample, 100 mL of pollutant solution (10 mg L^{-1}). Cr (VI) reduction: 300 W Xe lamp (λ ≥ 420 nm), 50 mg of sample, 100 mL of Cr (VI) solution (5 mg L^{-1})	Tetracyclines degradation: 2.01 h^{-1} Cr (VI) reduction: 2.412 h^{-1}	[68]
Same as above	Modify Co and Ni species	CO_2 reduction	300 W Xe lamp, H_2O as sacrificial agent.	≈2.4 μmol g^{-1} h^{-1} (CO)	[69]
Same as above	Modify Mn and Cu species	CO_2 reduction	300 W Xe lamp, H_2O as sacrificial agent.	≈2.3 μmol g^{-1} h^{-1} (CO)	[94]
Composite construction	Couple with NH_2-UiO-66(Zr)	CO_2 reduction	300 W Xe lamp (λ ≥ 400 nm), triethanolamine and H_2O as sacrificial agent.	31.7 μmol g^{-1} h^{-1} (CO)	[95]
Same as above	Combine with $Ba_5Nb_4O_{15}$	H_2 evolution	Four 3 W LED lamp (420 nm), oxalic acid as sacrificial agent, Pt as co-catalyst.	2670 μmol g^{-1} h^{-1}	[96]
Same as above	Combine with copper phosphide	H_2 evolution	Four 3 W LED lamp (420 nm), triethanolamine as sacrificial agent.	277.2 μmol g^{-1} h^{-1}	[97]

(*continued on next page*)

Table 2 (*continued*)

strategy	Method	Application	Reaction situation	Performance	Ref.
Same as above	Couple with nanodiamond	H_2 evolution	300 W Xe lamp ($\lambda \geq 420$ nm), triethanolamine as sacrificial agent, Pt as co-catalyst.	1182 μmol g^{-1} h^{-1}	[98]
Same as above	Modify Cu_2MoS_4	H_2 evolution	300 W Xe lamp ($\lambda \geq 420$ nm), triethanolamine as sacrificial agent.	2170.5 μmol g^{-1} h^{-1}	[99]
Same as above	Couple with perylene diimide	Phenol degradation, Oxygen evolution, *Staphylococcus aureus* disinfection	Phenol degradation: 500 W Xe lamp ($\lambda \geq 420$ nm), 25 mg of sample, 50 mL of pollutant solution (5 ppm). Oxygen evolution: 300 W Xe lamp ($\lambda \geq 420$ nm), 25 mg of sample, 100 mL of $AgNO_3$ solution (10 mM). *Staphylococcus aureus* disinfection: 00 W Xe lamp ($\lambda \geq 420$ nm), 0.2 g L^{-1} of photocatalyst, 1×10^7 cfu mL^{-1} of staphylococcus aureus.	Phenol degradation: 0.164 h^{-1} Oxygen evolution: 3.75 μmol at 2 h *Staphylococcus aureus* disinfection: ≈96.6 % at 3 h	[71]
Same as above	Combine with TiO_2 nanosheets	H_2 evolution	300 W Xe lamp, triethanolamine as sacrificial agent, Pt as co-catalyst.	18200 μmol g^{-1} h^{-1}	[100]
Same as above	Couple with NiAl-LDH	CO_2 reduction	300 W Xe lamp ($\lambda \geq 420$ nm), H_2O as sacrificial agent.	8.2 μmol g^{-1} h^{-1}	[101]
Same as above	Couple with TiO_2 meso-crystals	H_2 evolution	300 W Xe lamp with an AM 1.5 filter ($\lambda \geq 420$ nm), methanol as sacrificial agent.	1200 μmol g^{-1} h^{-1} (CO)	[102]
Same as above	Decorate cobalt (II) meso-tetraphenylporphine	H_2 evolution	300 W Xe lamp ($\lambda \geq 420$ nm), triethanolamine as sacrificial agent, Pt as co-catalyst.	938.6 μmol g^{-1} h^{-1}	[103]
Same as above	In-situ combine with nitrogen-doped hollow-TiO_2	H_2 evolution	300 W Xe lamp with an AM 1.5 filter ($\lambda \geq 420$ nm), methanol as sacrificial agent.	296.4 μmol g^{-1} h^{-1}	[104]
Same as above	Combine with oxygen vacancy rich TiO_2 quantum dots	CO_2 reduction	300 W Xe lamp ($\lambda \geq 400$ nm), 4 mL of methyl cyanide solvent, 1 mL of triethanolamine, 10 mmol/L bipyridine and 25 μL of 20 mmol/L $CoCl_2$ solution.	77.8 μmol g^{-1} h^{-1} (CO)	[105]
Same as above	Introduce 11,11,12,12-tetracyanonaphtho-1,4-quinodimethane	RhB degradation	500 W Xe lamp, 50 mg of sample, 50 mL of pollutant solution (10^{-5} mol L^{-1}).	≈19 h^{-1}	[106]
Same as above	Couple with covalent triazine-based frameworks	Sulfamethazine decomposition	500 W Xe lamp, 10 mg of sample, 50 mL of sulfamethazine solution (10 ppm).	95.8 % at 3 h	[72]
Same as above	Combine with one-dimensional Ni_2P-$Cd_{0.9}Zn_{0.1}S$	H_2 evolution	300 W Xe lamp ($\lambda \geq 420$ nm), Na_2S and Na_2SO_3 as sacrificial agent.	2100 μmol g^{-1} h^{-1}	[107]
Same as above	Combine with ZnO	RhB degradation	Sunlight irradiation, 0.1 g of photocatalyst, 100 mL of RhB solution (5 ppm).	99 % at 20 min	[108]
Same as above	Combine with Ti^{3+} doped TiO_2	RhB degradation	30 W LED lamp, 40 mg of photocatalyst, 10 mg L^{-1} RhB aqueous solution.	2.136 h^{-1}	[109]
Same as above	Couple with α-$Ni(OH)_2$	H_2 evolution	300 W Xe lamp ($\lambda \geq 400$ nm), triethanolamine as sacrificial agent, Pt as co-catalyst.	4764.9 μmol g^{-1} h^{-1}	[70]
Same as above	Combine with WO_3 and carbon dots	CO_2 reduction	300 W Xe lamp, H_2O as sacrificial agent.	31.04 μmol g^{-1} h^{-1}	[110]
Same as above	Couple with RGO and Bi_2WO_6	CO_2 reduction	300 W Xe lamp ($\lambda \geq 420$ nm), H_2O as sacrificial agent.	15.96 μmol g^{-1} h^{-1}	[111]
Same as above	Introduce CeO_2 quantum dots	Sterilization of *Staphylococcus aureus*	150 W Xe lamp ($\lambda \geq 420$ nm), 10 μg as prepared photocatalysts, 1 mL liquid bacterial broth (1×10^5 CFU per mL).	88.1 % at 15 min	[112]
Same as above	Couple with $MnIn_2S_4$	Tetracycline hydrochloride degradation, H_2 evolution	Tetracycline hydrochloride degradation: 30 mg of photocatalyst, 30 mL of tetracycline hydrochloride solution (50 mg L^{-1}). H_2 evolution: 300 W Xe lamp ($\lambda \geq 400$ nm), Na_2S and Na_2SO_3 as sacrificial agent.	Tetracycline hydrochloride degradation: ≈100 % at 90 min H_2 evolution: 200.8 μmol h^{-1} g^{-1}	[113]
Same as above	Combine with WO_3 nanosheets and load Pt	H_2 evolution	300 W Xe lamp ($\lambda \geq 420$ nm), triethanolamine as sacrificial agent.	17240 μmol h^{-1} g^{-1}	[75]
Same as above	Couple with $Ni(OH)_2$	H_2 evolution	300 W Xe lamp, triethanolamine as sacrificial agent.	4360 μmol h^{-1} g^{-1}	[114]
Same as above	Introduce CdS and Fe_3O_4	Tetracycline decomposition	300 W Xe lamp ($\lambda \geq 420$ nm), 100 mL of antibiotic solution (20 mg L^{-1}), 0.05 g of photocatalyst.	6.9 h^{-1}	[115]
Same as above	Couple with Cu_3P	H_2 evolution	300 W Xe lamp ($\lambda \geq 420$ nm), triethanolamine as sacrificial agent.	808 μmol h^{-1} g^{-1}	[116]
Same as above	Combine with Co_3O_4	H_2 evolution	300 W Xe lamp ($\lambda \geq 400$ nm), triethanolamine as sacrificial agent, Pt as co-catalyst.	37000 μmol g^{-1} h^{-1}	[117]
Same as above	Couple with oxygen defective ZnO nanorods	4-chlorophenol degradation, H_2 evolution	4-chlorophenol degradation: 300 W Xe lamp ($\lambda \geq 420$ nm), 0.1 g of the photocatalyst, 100 mL of 4-CP aqueous solution (10^{-4} mol L^{-1}).	4-chlorophenol degradation: 3.051 h^{-1} H_2 evolution: 322 μmol g^{-1} h^{-1}	[118]

(*continued on next page*)

Table 2 (*continued*)

strategy	Method	Application	Reaction situation	Performance	Ref.
			H_2 evolution: 300 W Xe lamp ($\lambda \geq 420$ nm), triethanolamine as sacrificial agent, Pt as co-catalyst.		
Same as above	Couple with CoAl-layered double hydroxide nanosheets	Methyl orange degradation	300 W Xe lamp ($\lambda \geq 420$ nm), 100 mL methyl orange solution (20 mg L^{-1}), 30 mg of photocatalyst.	5.74 h^{-1}	[119]
Same as above	Modify Pt and couple with WO_x	H_2 evolution, CO_2 reduction, Benzene oxidation	H_2 evolution: 300 W Xe lamp, triethanolamine as sacrificial agent. CO_2 reduction: 300 W Xe lamp ($\lambda \geq 420$ nm), H_2O as sacrificial agent. Benzene oxidation: 300 W Xe lamp ($\lambda \geq 420$ nm), 20 mg of photocatalyst, 6 mL of acetonitrile, 0.4 mL of benzene, and 6 mL of H_2O_2 (25 %).	H_2 evolution: 5267 μmol g^{-1} h^{-1} CO_2 reduction: 5.89 μmol g^{-1} h^{-1} (CO) and 3.12 μmol g^{-1} h^{-1} (CH_4) Benzene oxidation: 89.0 % at 12 h with the selectivity of 98.2 %	[120]
Same as above	Decorate Ni and couple with Bi_2WO_6	Photothermal conversion of CO_2 and H_2O to syngas	300 W Xe lamp, heating temperature of 250 °C.	4493 μmol g^{-1} h^{-1} (CO), 9191 μmol g^{-1} h^{-1} (H_2)	[73]
Same as above	Anchor nickel stannate perovskite	H_2 evolution	Two tungsten-halogen lamps (250 W each), triethanolamine as sacrificial agent, Pt as co-catalyst.	646 μmol g^{-1} h^{-1}	[121]
Same as above	Couple with $ZnIn_2S_4$	H_2 evolution	300 W Xe lamp ($\lambda \geq 420$ nm), triethanolamine as sacrificial agent, Pt as co-catalyst.	1650 μmol g^{-1} h^{-1}	[122]
Same as above	Introduce Ta^{4+} doped Ta_2O_5 quantum dots	H_2 evolution, RhB degradation	H_2 evolution: 300 W Xe lamp ($\lambda \geq 420$ nm), triethanolamine as sacrificial agent, Pt as co-catalyst. RhB degradation: 300 W Xe lamp ($\lambda \geq 420$ nm), 0.1 g of photocatalyst, 10 mg L^{-1} of RhB solution.	H_2 evolution: 624.99 μmol g^{-1} h^{-1}, RhB degradation:9.072 h^{-1}	[123]
Same as above	Couple with Cu_2MoS_4 nanosheets	H_2 evolution	300 W Xe lamp ($\lambda \geq 400$ nm), Na_2S and Na_2SO_3 as sacrificial agent.	2385 μmol g^{-1} h^{-1}	[124]
Same as above	Introduce CdS and MoS_2	RhB degradation	300 W Xe lamp ($\lambda \geq 420$ nm), 0.01 g of photocatalyst, 50 mL of RhB solution (10 mM).	3.198 h^{-1}	[77]
Same as above	Combine with BiOI and AgI	Tetracycline degradation	300 W Xe lamp ($\lambda \geq 420$ nm), 50 mg of photocatalyst, 50 mL of tetracycline solution (20 mg L^{-1}).	2.334 h^{-1}	[125]
Same as above	Introduce CoO and Co_3O_4	Nitrobenzene degradation, Tetracycline degradation	Nitrobenzene degradation: 500 W Xeon lamp, 30 mg of photocatalyst, 50 mL of nitrobenzene solution (5 mg L^{-1}). Tetracycline degradation: 500 W Xeon lamp, 30 mg of photocatalyst, 50 mL of tetracycline solution (10 mg L^{-1}).	Nitrobenzene degradation: 1.02 h^{-1} Tetracycline degradation: 1.26 h^{-1}	[126]
Same as above	Couple with MIL-53(Fe) and α-Bi_2O_3	Amido black 10 B degradation	35 W Xenon lamp, 20 mg of photocatalyst, 50 mL of amido black 10 B (10 mg L^{-1}).	5.06 h^{-1}	[127]
Same as above	Combine with Ag_3PO_4 and AgI	NTP degradation, RhB degradation	NTP degradation: 300 W Xe lamp ($\lambda \geq 420$ nm), 25 mg of photocatalyst, 50 mL of NTP solution (5 ppm). RhB degradation: 300 W Xe lamp ($\lambda \geq 420$ nm), 25 mg of photocatalyst, 50 mL of RhB solution (20 ppm).	NTP degradation: 45.6 h^{-1} RhB degradation: 22.8 h^{-1}	[78]
Same as above	Introduce $CeCO_3OH$ and CeO_2	nitrogen fixation	500 W Xenon lamp, 30 mg of the photocatalyst, water as sacrificial agent.	1160 μmol g^{-1} h^{-1}	[79]

3.2. Composite construction

Viewed through the perspective of prolonging the charge carrier lifetime in g-C_3N_4 by promoting the spatial separation of photoexcited electron-hole pairs, building composite structure with other semiconductors presents a promising strategy that enables the efficient transfer of charge carriers across the compounds. Owing to the negative positions of the conduction and valence bands of g-C_3N_4, scholarly research concerning composite-construction predominantly concentrate on the type-II and Z-scheme structures (as shown in Fig. 9).

In the type-II mechanism, electrons from the surface of material A spontaneously transfer to material B, for which the conduction band of material A is more negative than B. Meanwhile, the holes from the surface of material B transfer to material A, for which the valence band of material B is more positive than A. Consequently, the electrons and holes will be located on different components of the composite, thereby suppressing the recombination of the charge carriers, and prolonging their lifetime. The works focus on the type-II structure have thus been reported. Yang et al. [70] fabricated $Ni(OH)_2$/g-C_3N_4 nanocomposite through an in-situ growth approach. Through DFT calculations, electron paramagnetic resonance, photoluminescence spectroscopy, time-resolved fluorescence decay spectroscopy, electrochemical impedance spectroscopy and electrochemical analyses, it has been demonstrated that the photo-generated electrons from $Ni(OH)_2$ are transferred to the conduction band of g-C_3N_4, concurrently, the photo-induced holes from g-C_3N_4 migrate to the valence band of $Ni(OH)_2$, thereby result in an promoted charge separation and an prolonged charge lifetime. Gao et al. [71] introduced self-assembled perylene diimide nanofibers onto the surface of g-C_3N_4 through an in-situ method. Through a comprehensive suite of analytical techniques, including photoelectrochemical analysis, electrochemical impedance spectroscopy, surface photovoltage spectroscopy, photoluminescence spectroscopy, time-resolved fluorescence decay spectroscopy, and electron spin resonance technique, it has been illustrated that the composite exhibits superior charge separation capabilities compared to pristine g-C_3N_4, a phenomenon attributed to the enhanced lifetime of charge carriers facilitated by the type-II charge transfer mechanism. Cao and the co-workers fabricate the composite consist of covalent triazine-based frameworks and g-C_3N_4 via a wet-chemical method [72]. From the results of charge separation property related measurements, including photoelectrochemical analysis, electrochemical impedance spectroscopy, photoluminescence spectroscopy, time-resolved fluorescence decay spectroscopy, and electron spin resonance, it has been elucidated that g-C_3N_4-generated photo-electrons are transferred to the conduction band of covalent triazine-based frameworks, whereas the holes migrate in a reverse fashion. This charge transfer process significantly augments the photo-induced charge separation efficiency and extends the life of charge carriers.

In the Z-scheme mechanism, electrons on the surface of material B, which has a more positive conduction band, recombine with holes on the surface of material A, which has a more negative valence band. As a result, the electrons and holes with higher energy are left separated on materials A and B. This spatial separation effectively prolongs the lifetimes of the electrons and holes. Some studies focusing on the Z-scheme have thus been carried out. Wu et al. [73] synthesized a composite of g-C_3N_4 and Bi_2WO_6 employing an in-situ growth strategy, which encompasses a sequential hydrothermal procedure followed by a calcination process. As evidenced by a suite of techniques, including electron paramagnetic resonance spin, X-ray photoelectron spectroscopy, photoluminescence spectroscopy, Nyquist analysis, transient photocurrent measurement, and time-resolved fluorescence spectroscopy, it has been confirmed that a Z-scheme heterojunction is successfully fabricated, in which the photo-holes generated by g-C_3N_4 recombine with the photo-electrons generated by Bi_2WO_6, thereby facilitating the preservation of charge carriers with high energy and prolong their lifetime. Xu et al. [74] have successfully fabricated a composite consisting of perylene diimide and g-C_3N_4 for the purpose of cleaving lignin models. The composite was synthesized via a facile solvent evaporation wet-chemical method. The results of DFT calculations and measurements related to charge separation and transfer behavior, encompassing transient photocurrent response, electrochemical impedance spectroscopy, time-resolved fluorescence decay spectroscopy, and electron spin resonance, reveal that the enhancement of charge separation can be attributed to the Z-scheme charge transfer process which effectively prolongs the lifetime of photogenerated charge carriers. Liu et al. [75] successfully synthesized a compound comprising of WO_3 and g-C_3N_4 through a wet-chemical method, with the aim of generating H_2. Various characterization techniques, including electron spin resonance, photoluminescence spectroscopy, UV-vis adsorption spectroscopy, electrochemical impedance spectroscopy, photo-induced current density test, and time-dependent fluorescence decay responses, were employed to investigate the charge separation and carrier lifetime properties of the composite. The experimental results demonstrate that the composite exhibits enhanced charge separation and prolonged lifetime of charge carriers compared to pristine g-C_3N_4. The mechanism underlying this enhancement has been identified as the Z-scheme, wherein electrons generated by WO_3 can recombine with holes generated by g-C_3N_4, while leaving electrons and holes separately localized on the surfaces of g-C_3N_4 and WO_3.

Many studies have also focused on constructing ternary compound systems, such as dual type-II composites and dual Z-scheme composites. These approaches aim to achieve improved separation of photogenerated electron-hole pairs. Yang et al. [76] employed a facile impregnation method to introduce WS_2 and TiO_2 onto the surface of g-C_3N_4. Through a comprehensive analysis including electron paramagnetic resonance measurement, photoluminescence spectroscopy, time-resolved fluorescence measurement, electrochemical impedance spectroscopy, and transient photocurrent response, they demonstrated that the co-introduction of WS_2 and TiO_2 effectively enhances charge separation and prolongs charge lifetime by establishing a type-II charge separation mechanism. Zhang et al. [77] utilized a simple wet-chemical method to fabricate a composite consisting of MoS_2, CdS, and g-C_3N_4. This composite exhibited enhanced charge separation properties due to the formation of a dual type-II charge transfer mechanism. Tang et al. [78] employed an in-situ ion exchange method to simultaneously combine Ag_3PO_4 and AgI on g-C_3N_4. Through various charge separation-related experimental techniques, such as photoluminescence spectroscopy, transient photocurrent measurement, electrochemical impedance spectroscopy, electron spin resonance measurement, and radical-related fluorescence spectroscopy, they demonstrated that the composite exhibits enhanced charge separation properties compared to the pristine material. This enhancement

is attributed to the photogenerated charge carriers transferring through a dual Z-scheme mechanism. In their study, Feng et al. [79] successfully synthesized a composite of $CeCO_3OH$, CeO_2 and g-C_3N_4 using a facile in-situ self-sacrificing hydrothermal method for photocatalytic nitrogen fixation. Through analyses including photocurrent spectroscopy, time-resolved fluorescence spectroscopy, and electron paramagnetic resonance measurement, they discovered that the prolonged lifetime of charge carriers can be attributed to the formation of a dual Z-scheme mechanism consisting of $CeCO_3OH$/g-C_3N_4 and CeO_2/g-C_3N_4 in the composite.

Several related works about promoting charge separation property of g-C_3N_4 by the above-mentioned strategies have been summarized in Table 2.

4. Conclusions and perspectives

Over the past few years, g-C_3N_4 has received significant attention as a promising photocatalyst for its beneficial properties, such as non-metal component, low cost, earth abundant, and two-dimension structure. Nonetheless, the unsatisfactory charge separation property hinders its photocatalytic performance. This review systematically categorizes the methods aimed at enhancing the charge separation property of g-C_3N_4. These strategies can be categorized into two major directions: promoting the surface migration of charge carriers and prolonging the lifetime of surface charge carriers. Despite significant efforts, the application of g-C_3N_4-based photocatalytic materials in industrial settings is still a distant prospect. Hence, we propose several potential reference schemes aimed at enhancing charge separation to facilitate the further development of g-C_3N_4-based photocatalytic materials.

(1) Indeed, achieving a high specific surface area is crucial for promoting charge separation in g-C_3N_4. The theoretical specific surface area of g-C_3N_4 can reach 2500 m^2/g, while existing methods struggle to achieve such levels. Therefore, it is necessary to develop simple preparation strategies that enable the preparation of g-C_3N_4 with a very high specific surface area. Currently, g-C_3N_4 preparation is mainly based on the polymerization reaction of small precursor molecules, which is a bottom-up synthesis process that is difficult to control. However, recent works have shown that self-assembly of the precursor can improve the specific surface area by transforming the process into a top-down approach and effectively increased the surface area. Nevertheless, in this self-assembly process, there is an issue of imbalanced transformation from bulk to nanosheets, leading to the decomposition of some of the transformed g-C_3N_4 nanosheets. This limitation hinders the effective expansion of the specific surface area. To overcome this challenge, adjusting the size of the precursors could potentially help achieve a more balanced transformation process, facilitating the transition from blocks to nanosheets and solving this problem.

(2) In the current complex construction strategies, the construction of a type II structure may result in the sacrifice of electron and hole energy, and electrons can still recombine with holes through the Z-type path. Additionally, in the Z-type structure, electrons tend to spontaneously transfer to the band position with lower energy. This means that the residual electrons on A in Fig. 9 can easily transfer to the conduction band of B and subsequently recombine with holes, thereby affecting the effective promotion of charge separation. To conquer this challenge, it is significant to develop a more effective composite model to achieve effective spatial separation of photogenerated electrons and holes, such as accelerating charge transfer between composites through constructing electron bridges, constructing multiple heterojunctions, and surface engineering.

CRediT authorship contribution statement

Shuangying Chen: Writing – original draft, Investigation, Formal analysis, Conceptualization. **Xuliang Zhang:** Writing – review & editing, Supervision, Funding acquisition. **Degang Li:** Writing – review & editing. **Xiaowen Wang:** Writing – review & editing. **Bingjie Hu:** Writing – review & editing. **Fushui Guo:** Writing – review & editing. **Liantao Hao:** Writing – review & editing. **Bo Liu:** Writing – review & editing.

Declaration of competing interest

The authors declare that they have no known competing financial interests or personal relationships that could have appeared to influence the work reported in this paper.

Acknowledgments

We are grateful for financial support from the National Natural Science Foundation of China (22002074), Natural Science Foundation of Shandong Province (ZR2022ME010).

References

[1] T. Jeong, H. Piao, S. Park, J.-H. Yang, G. Choi, Q. Wu, H. Kang, H.J. Woo, S.J. Jung, H. Kim, B.G. Shin, Y. Kim, E.H. Hwang, J.-H. Choy, Y.J. Song, Atomic and electronic structures of graphene-decorated graphitic carbon nitride (g-C_3N_4) as a metal-free photocatalyst under visible-light, Appl. Catal. B Environ. 256 (2019) 117850.

[2] D.J. Martin, K. Qiu, S.A. Shevlin, A.D. Handoko, X. Chen, Z. Guo, J. Tang, Highly efficient photocatalytic H_2 evolution from water using visible light and structure-controlled graphitic carbon nitride, Angew. Chem. Int. Ed. 53 (2014) 9240–9245.

[3] H. Wang, Y. Xu, D. Xu, L. Chen, X. Qiu, Y. Zhu, Graphitic carbon nitride for photoelectrochemical detection of environmental pollutants, ACS ES&T Engineering 2 (2022) 140–157.

[4] J. Wang, C. Qin, H. Wang, M. Chu, A. Zada, X. Zhang, J. Li, F. Raziq, Y. Qu, L. Jing, Exceptional photocatalytic activities for CO_2 conversion on Al-O bridged g-C_3N_4/α-Fe_2O_3 z-scheme nanocomposites and mechanism insight with isotopes, Appl. Catal. B Environ. 221 (2018) 459–466.
[5] C. Wu, S. Xue, Z. Qin, M. Nazari, G. Yang, S. Yue, T. Tong, H. Ghasemi, F.C.R. Hernandez, S. Xue, D. Zhang, H. Wang, Z.M. Wang, S. Pu, J. Bao, Making g-C_3N_4 ultra-thin nanosheets active for photocatalytic overall water splitting, Appl. Catal. B Environ. 282 (2021) 119557.
[6] Y. Yu, H. Huang, Coupled adsorption and photocatalysis of g-C_3N_4 based composites: material synthesis, mechanism, and environmental applications, Chem. Eng. J. 453 (2023) 139755.
[7] A. Fujishima, K. Honda, Electrochemical photolysis of water at a semiconductor electrode, Nature 238 (1972) 37–38.
[8] M. Gu, Y. Yang, L. Zhang, B. Zhu, G. Liang, J. Yu, Efficient sacrificial-agent-free solar H_2O_2 production over all-inorganic S-scheme composites, Appl. Catal. B Environ. 324 (2023) 122227.
[9] K. Jiang, W. Huang, T. Song, P. Wu, W. Wang, Q. Chen, M. Wang, G. Guo, Photobreeding heterojunction on semiconductor materials for enhanced photocatalysis, Adv. Funct. Mater. 33 (2023) 2304351.
[10] F. Li, X. Yue, Y. Liao, L. Qiao, K. Lv, Q. Xiang, Understanding the unique S-scheme charge migration in triazine/heptazine crystalline carbon nitride homojunction, Nat. Commun. 14 (2023) 3901.
[11] X. Wang, K. Maeda, A. Thomas, K. Takanabe, G. Xin, J.M. Carlsson, K. Domen, M. Antonietti, A metal-free polymeric photocatalyst for hydrogen production from water under visible light, Nat. Mater. 8 (2008) 76–80.
[12] S. Stefa, M. Griniezaki, M. Dimitropoulos, G. Paterakis, C. Galiotis, G. Kiriakidis, E. Klontzas, M. Konsolakis, V. Binas, Highly porous thin-layer g-C_3N_4 nanosheets with enhanced adsorption capacity, ACS Appl. Nano Mater. 6 (2023) 1732–1743.
[13] B. Qu, P. Li, L. Bai, Y. Qu, Z. Li, Z. Zhang, B. Zheng, J. Sun, L. Jing, Atomically dispersed Zn-N_5 sites immobilized on g-C_3N_4 nanosheets for ultrasensitive selective detection of phenanthrene by dual ratiometric fluorescence, Adv. Mater. 35 (2023) 2211575.
[14] L. Du, B. Gao, S. Xu, Q. Xu, Strong ferromagnetism of g-C_3N_4 achieved by atomic manipulation, Nat. Commun. 14 (2023) 2278.
[15] P. Niu, J. Dai, X. Zhi, Z. Xia, S. Wang, L. Li, Photocatalytic overall water splitting by graphitic carbon nitride, InfoMat 3 (2021) 931–961.
[16] H. Wang, X. Liu, P. Niu, S. Wang, J. Shi, L. Li, Porous two-dimensional materials for photocatalytic and electrocatalytic applications, Matter 2 (2020) 1377–1413.
[17] X. Zhang, H.S. Chen, S.P. Jiang, P. Yang, $W_{18}O_{49}$/crystalline g-C_3N_4 layered heterostructures with full solar energy harvesting towards efficient H_2O_2 generation and NO conversion, Nano Energy 120 (2024) 109160.
[18] G. Liao, Y. Gong, L. Zhang, H. Gao, G.-J. Yang, B. Fang, Semiconductor polymeric graphitic carbon nitride photocatalysts: the "Holy Grail" for the photocatalytic hydrogen evolution reaction under visible light, Energy Environ. Sci. 12 (2019) 2080–2147.
[19] Y. Ni, R. Wang, W. Zhang, S. Shi, W. Zhu, M. Liu, C. Yang, X. Xie, J. Wang, Graphitic carbon nitride (g-C_3N_4)-based nanostructured materials for photodynamic inactivation: synthesis, efficacy and mechanism, Chem. Eng. J. 404 (2021) 126528.
[20] L. Wang, K. Wang, T. He, Y. Zhao, H. Song, H. Wang, Graphitic carbon nitride-based photocatalytic materials: preparation strategy and application, ACS Sustain. Chem. Eng. 8 (2020) 16048–16085.
[21] X. Zhang, K. Zhu, C. Xie, P. Yang, Vertically implanting $MoSe_2$ nanosheets on superior thin C-doped g-C_3N_4 nanosheets towards interface-enhanced electrochemical activities, Carbon 220 (2024) 118884.
[22] X. Zhang, P. Yang, Role of graphitic carbon in g-C_3N_4 nanoarchitectonics towards efficient photocatalytic reaction kinetics: a review, Carbon 216 (2024) 118584.
[23] T. Song, X. Zhang, C. Xie, P. Yang, N-doped carbon nanotubes enhanced charge transport between Ni nanoparticles and g-C_3N_4 nanosheets for photocatalytic H_2 generation and 4-nitrophenol removal, Carbon 210 (2023) 118052.
[24] X. Zhang, P. Yang, H.S. Chen, S.P. Jiang, Carbon layer derived carrier transport in Co/g-C_3N_4 nanosheet junctions for efficient H_2O_2 production and NO removal, Chem. Eng. J. 479 (2024) 147609.
[25] C. Merschjann, S. Tschierlei, T. Tyborski, K. Kailasam, S. Orthmann, D. Hollmann, T. Schedel-Niedrig, A. Thomas, S. Lochbrunner, Complementing graphenes: 1D interplanar charge transport in polymeric graphitic carbon nitrides, Adv. Mater. 27 (2015) 7993–7999.
[26] H. Wang, S. Jiang, S. Chen, X. Zhang, W. Shao, X. Sun, Z. Zhao, Q. Zhang, Y. Luo, Y. Xie, Insights into the excitonic processes in polymeric photocatalysts, Chem. Sci. 8 (2017) 4087–4092.
[27] S. Brazovskii, N. Kirova, Physical theory of excitons in conducting polymers, Chem. Soc. Rev. 39 (2010) 2453–2465.
[28] A.J. Heeger, Semiconducting polymers: the third generation, Chem. Soc. Rev. 39 (2010) 2354–2371.
[29] H. Gao, R. Cao, S. Zhang, H. Yang, X. Xu, Three-dimensional hierarchical g-C_3N_4 architectures assembled by ultrathin self-doped nanosheets: extremely facile hexamethylenetetramine activation and superior photocatalytic hydrogen evolution, ACS Appl. Mater. Interfaces 11 (2019) 2050–2059.
[30] Z. Zeng, X. Quan, H. Yu, S. Chen, S. Zhang, Nanoscale lightning rod effect in 3D carbon nitride nanoneedle: enhanced charge collection and separation for efficient photocatalysis, J. Catal. 375 (2019) 361–370.
[31] J. Mao, L. Zhang, H. Wang, Q. Zhang, W. Zhang, P. Li, Facile fabrication of nanosized graphitic carbon nitride sheets with efficient charge separation for mitigation of toxic pollutant, Chem. Eng. J. 342 (2018) 30–40.
[32] B. Li, Y. Si, B.-X. Zhou, Q. Fang, Y.-Y. Li, W.-Q. Huang, W. Hu, A. Pan, X. Fan, G.-F. Huang, Doping-induced hydrogen-bond engineering in polymeric carbon nitride to significantly boost the photocatalytic H_2 evolution performance, ACS Appl. Mater. Interfaces 11 (2019) 17341–17349.
[33] Q. Yang, Z. Li, C. Chen, Z. Zhang, X. Fang, Enhanced charge separation and transport efficiency induced by vertical slices on the surface of carbon nitride for visible-light-driven hydrogen evolution, RSC Adv. 9 (2019) 4404–4414.
[34] C. Liu, Y. Zhang, F. Dong, X. Du, H. Huang, Easily and synchronously ameliorating charge separation and band energy level in porous g-C_3N_4 for boosting photooxidation and photoreduction ability, J. Phys. Chem. C 120 (2016) 10381–10389.
[35] J. Xu, Z. Wang, Y. Zhu, Enhanced visible-light-driven photocatalytic disinfection performance and organic pollutant degradation activity of porous g-C_3N_4 nanosheets, ACS Appl. Mater. Interfaces 9 (2017) 27727–27735.
[36] L. Yin, S. Wang, C. Yang, S. Lyu, X. Wang, Modulation of polymeric carbon nitrides through supramolecular preorganization for efficient photocatalytic hydrogen generation, ChemSusChem 12 (2019) 3320–3325.
[37] C. Liu, H. Huang, L. Ye, S. Yu, N. Tian, X. Du, T. Zhang, Y. Zhang, Intermediate-mediated strategy to horn-like hollow mesoporous ultrathin g-C_3N_4 tube with spatial anisotropic charge separation for superior photocatalytic H_2 evolution, Nano Energy 41 (2017) 738–748.
[38] C. Merschjann, S. Tschierlei, T. Tyborski, K. Kailasam, S. Orthmann, D. Hollmann, T. Schedel-Niedrig, A. Thomas, S. Lochbrunner, Complementing graphenes: 1D interplanar charge transport in polymeric graphitic carbon nitrides, Adv. Mater. 27 (2015) 7993–7999.
[39] Z. Chen, T. Fan, M. Shao, X. Yu, Q. Wu, J. Li, W. Fang, X. Yi, Simultaneously enhanced photon absorption and charge transport on a distorted graphitic carbon nitride toward visible light photocatalytic activity, Appl. Catal. B Environ. 242 (2019) 40–50.
[40] H. Shi, S. Long, J. Hou, L. Ye, Y. Sun, W. Ni, C. Song, K. Li, G.G. Gurzadyan, X. Guo, Defects promote ultrafast charge separation in graphitic carbon nitride for enhanced visible-light-driven CO_2 reduction activity, Chem.–Eur. J. 25 (2019) 5028–5035.
[41] J. Kang, W. Ha, H. Zhang, Y. Shi, Sandwich-like, potassium(I) doped g-C_3N_4 with tunable interlayer distance as a high selective extractant for the determination of Ba(II), Talanta 215 (2020) 120916.
[42] T. Xiong, W. Cen, Y. Zhang, F. Dong, Bridging the g-C_3N_4 interlayers for enhanced photocatalysis, ACS Catal. 6 (2016) 2462–2472.
[43] J. Li, W. Cui, Y. Sun, Y. Chu, W. Cen, F. Dong, Directional electron delivery via a vertical channel between g-C_3N_4 layers promotes photocatalytic efficiency, J. Mater. Chem. A 5 (2017) 9358–9364.
[44] T. Xiong, H. Wang, Y. Zhou, Y. Sun, W. Cen, H. Huang, Y. Zhang, F. Dong, KCl-mediated dual electronic channels in layered g-C_3N_4 for enhanced visible light photocatalytic NO removal, Nanoscale 10 (2018) 8066–8074.
[45] W. Cui, J. Li, W. Cen, Y. Sun, S.C. Lee, F. Dong, Steering the interlayer energy barrier and charge flow via bioriented transportation channels in g-C_3N_4: enhanced photocatalysis and reaction mechanism, J. Catal. 352 (2017) 351–360.

[46] S. Bellamkonda, R. Shanmugam, R.R. Gangavarapu, Extending the pi-electron conjugation in 2D planar graphitic carbon nitride: efficient charge separation for overall water splitting, J. Mater. Chem. A 7 (2019) 3757–3771.

[47] Z. Liang, Y. Xia, G. Ba, H. Li, Q. Deng, W. Hou, Facile synthesis of tin-doped polymeric carbon nitride with a hole-trapping center for efficient charge separation and photocatalytic hydrogen evolution, J. Mater. Chem. A 7 (2019) 25824–25829.

[48] C. Yang, Z. Xue, J. Qin, M. Sawangphruk, X. Zhang, R. Liu, Heterogeneous structural defects to prompt charge shuttle in g-C_3N_4 plane for boosting visible-light photocatalytic activity, Appl. Catal. B Environ. 259 (2019).

[49] Z. Liang, Y. Xia, G. Ba, H. Li, Q. Deng, W. Hou, Sb-doped polymeric carbon nitride with charge-capture centers for efficient charge separation and photocatalytic performance in H_2 evolution and environmental remediation, Catal. Sci. Technol. 9 (2019) 6627–6637.

[50] G. Ba, Z. Liang, H. Li, Q. Deng, N. Du, W. Hou, Synthesis of hierarchically mesoporous polymeric carbon nitride with mesoporous melamine as a precursor for enhanced photocatalytic performance, Chem. Eng. J. 380 (2020) 122535.

[51] Y. Xiao, G. Tian, W. Li, Y. Xie, B. Jiang, C. Tian, D. Zhao, H. Fu, Molecule self-assembly synthesis of porous few-layer carbon nitride for highly efficient photoredox catalysis, J. Am. Chem. Soc. 141 (2019) 2508–2515.

[52] S. Cao, H. Li, T. Tong, H.-C. Chen, A. Yu, J. Yu, H.M. Chen, Single-atom engineering of directional charge transfer channels and active sites for photocatalytic hydrogen evolution, Adv. Funct. Mater. 28 (2018) 1802169.

[53] H. Ou, S. Ning, P. Zhu, S. Chen, A. Han, Q. Kang, Z. Hu, J. Ye, D. Wang, Y. Li, Carbon nitride photocatalysts with integrated oxidation and reduction atomic active centers for improved CO_2 conversion, Angew. Chem. Int. Ed. 61 (2022) e202206579.

[54] Y. Wang, X. Liu, J. Liu, B. Han, X. Hu, F. Yang, Z. Xu, Y. Li, S. Jia, Z. Li, Y. Zhao, Carbon quantum dot implanted graphite carbon nitride nanotubes: excellent charge separation and enhanced photocatalytic hydrogen evolution, Angew. Chem. Int. Ed. 57 (2018) 5765–5771.

[55] H. Kim, S. Gim, T.H. Jeon, H. Kim, W. Choi, Distorted carbon nitride structure with substituted benzene moieties for enhanced visible light photocatalytic activities, ACS Appl. Mater. Interfaces 9 (2017) 40360–40368.

[56] X. Fang, L. Ma, K. Liang, S. Zhao, Y. Jiang, C. Ling, T. Zhao, T. Cheang, A. Xu, The doping of phosphorus atoms into graphitic carbon nitride for highly enhanced photocatalytic hydrogen evolution, J. Mater. Chem. A 7 (2019) 11506–11512.

[57] H. Li, Y. Xia, T. Hu, Q. Deng, N. Du, W. Hou, Enhanced charge carrier separation of manganese(II)-doped graphitic carbon nitride: formation of N-Mn bonds through redox reactions, J. Mater. Chem. A 6 (2018) 6238–6243.

[58] Y. Yao, Y. Wang, T. Lu, J. Zhang, K. Hu, H. Zhang, T. Pukala, Y. Liu, X. Duan, S. Wang, In-plane implanting carbon rings into carbon nitride to intrigue nonradical photodegradation, Appl. Catal. B Environ. 342 (2024) 123363.

[59] G. Zeng, D. Huang, C. Zhang, D. He, C. Zhou, W. Wang, W. Xiong, X. Li, B. Li, W. Dong, Y. Zhou, Molecular engineering of polymeric carbon nitride for highly efficient photocatalytic oxytetracycline degradation and H_2O_2 production, Appl. Catal. B Environ. 272 (2020) 118970.

[60] H. Zhang, J. Lin, Z. Li, T. Li, X. Jia, X.-L. Wu, S. Hu, H. Lin, J. Chen, J. Zhu, Organic dye doped graphitic carbon nitride with a tailored electronic structure for enhanced photocatalytic hydrogen production, Catal. Sci. Technol. 9 (2019) 502–508.

[61] W. Yan, Y. Yu, H. Zou, X. Wang, P. Li, W. Gao, J. Wang, S. Wu, K. Ding, Promoted photocatalytic hydrogen evolution by molecular ring-substituting doping and regulation of charge carrier migration in graphitic carbon nitride, Sol. RRL 2 (2018) 201800058.

[62] Y. Wang, X. Bai, H. Qin, F. Wang, Y. Li, X. Li, S. Kang, Y. Zuo, L. Cui, Facile one-step synthesis of hybrid graphitic carbon nitride and carbon composites as high-performance catalysts for CO_2 photocatalytic conversion, ACS Appl. Mater. Interfaces 8 (2016) 17212–17219.

[63] Y. Wang, Y. Qu, B. Qu, L. Bai, Y. Liu, Z.-D. Yang, W. Zhang, L. Jing, H. Fu, Construction of six-oxygen-coordinated single ni sites on g-C_3N_4 with boron-oxo species for photocatalytic water-activation-induced CO_2 reduction, Adv. Mater. 33 (2021) 2105482.

[64] C. Xue, P. Wang, H. Che, W. Liu, B. Liu, Y. Ao, Simultaneous organic pollutant degradation and hydrogen peroxide production by molecular-engineered carbon nitride, Appl. Catal. B Environ. 340 (2024) 123259.

[65] Y. Liu, X. Zhou, C. Shen, Z. Zhao, Y. Jiang, L. Ma, X. Fang, Z. Akif, T. Cheag, A. Xu, Hydrogen-bonding-assisted charge transfer: significantly enhanced photocatalytic H_2 evolution over g-C_3N_4 anchored with ferrocene-based hole relay, Catal. Sci. Technol. 8 (2018) 2853–2859.

[66] J. Li, X. Zhang, F. Raziq, J. Wang, C. Liu, Y. Liu, J. Sun, R. Yan, B. Qu, C. Qin, L. Jing, Improved photocatalytic activities of g-C_3N_4 nanosheets by effectively trapping holes with halogen-induced surface polarization and 2,4-dichlorophenol decomposition mechanism, Appl. Catal. B Environ. 218 (2017) 60–67.

[67] X. Zeng, Y. Liu, Y. Kang, Q. Li, Y. Xia, Y. Zhu, H. Hou, M.H. Uddin, T.R. Gengenbach, D. Xia, C. Sun, D.T. Mccarthy, A. Deletic, J. Yu, X. Zhang, Simultaneously tuning charge separation and oxygen reduction pathway on graphitic carbon nitride by polyethylenimine for boosted photocatalytic hydrogen peroxide production, ACS Catal. 10 (2020) 3697–3706.

[68] K. Ren, M. Lv, Q. Xie, C. Zhang, H. Shi, Dual BN quantum dot/Ag co-catalysts synergistically promote electron-hole separation on g-C_3N_4 nanosheets for efficient antibiotics oxidation and Cr(VI) reduction, Carbon 186 (2022) 355–366.

[69] X. Zhang, X. Zhang, W. Ali, X. Chen, K. Hu, Z. Li, Y. Qu, L. Bai, Y. Gao, L. Jing, Improved photoactivities of large-surface-area g-C_3N_4 for CO_2 conversion by controllably introducing Co- and Ni-species to effectively modulate photogenerated charges, ChemCatChem 11 (2019) 6282–6287.

[70] D. Yang, C. Qu, F. Meng, L. Meng, Y. Meng, Q. Ye, Synergistic enhancement of photocatalytic hydrogen evolution by ultrathin oxygen-doped graphitic carbon nitride nanosheets loaded amorphous mesoporous nickel hydroxide, Separ. Purif. Technol. 330 (2024) 125366.

[71] Q. Gao, J. Xu, Z. Wang, Y. Zhu, Enhanced visible photocatalytic oxidation activity of perylene diimide/g-C_3N_4 n-n heterojunction via pi-pi interaction and interfacial charge separation, Appl. Catal. B Environ. 271 (2020) 118933.

[72] S. Cao, Y. Zhang, N. He, J. Wang, H. Chen, F. Jiang, Metal-free 2D/2D heterojunction of covalent triazine-based frameworks/graphitic carbon nitride with enhanced interfacial charge separation for highly efficient photocatalytic elimination of antibiotic pollutants, J. Hazard Mater. 391 (2020) 122204.

[73] J. Wu, K. Li, S. An, S. Yan, J. Liu, C. Song, X. Guo, An S-scheme heterojunction of single Ni sites decorated ultrathin carbon nitride and Bi_2WO_6 for highly efficient photothermal CO_2 conversion to syngas, Appl. Catal., B: Environment and Energy 347 (2024) 123822.

[74] X. Xu, S. Dai, S. Xu, Q. Zhu, Y. Li, Efficient photocatalytic cleavage of lignin models by a soluble perylene diimide/carbon nitride S-scheme heterojunction, Angew. Chem. Int. Ed. 62 (2023) 202309066.

[75] D. Liu, S. Zhang, J. Wang, T. Peng, R. Li, Direct Z-scheme 2D/2D photocatalyst based on ultrathin g-C3N4 and WO3 nanosheets for efficient visible-light-driven H2 generation, ACS Appl. Mater. Interfaces 11 (2019) 27913–27923.

[76] C. Yang, J. Qin, S. Rajendran, X. Zhang, R. Liu, WS_2 and C-TiO_2 nanorods acting as effective charge separators on g-C_3N_4 to boost visible-light activated hydrogen production from seawater, ChemSusChem 11 (2018) 4077–4085.

[77] D. Zhang, T. Xu, M. Cao, A. Liu, Q. Zhao, L. Zhang, H. Zhang, T. Xue, X. Cui, W. Zheng, Facile band alignment of C_3N_4/CdS/MoS_2 sandwich hybrid for efficient charge separation and high photochemical performance under visible-light, Powder Technol. 351 (2019) 222–228.

[78] M. Tang, Y. Ao, C. Wang, P. Wang, Facile synthesis of dual Z-scheme g-C_3N_4/Ag_3PO_4/AgI composite photocatalysts with enhanced performance for the degradation of a typical neonicotinoid pesticide, Appl. Catal. B Environ. 268 (2020) 118395.

[79] X. Feng, H. Chen, F. Jiang, X. Wang, One-pot fabrication of a double Z-scheme $CeCO_3OH$/g-C_3N_4/CeO_2 photocatalyst for nitrogen fixation under solar irradiation, Catal. Sci. Technol. 9 (2019) 2849–2857.

[80] B. Kousik, C. Moumita, K. Santimoy, P. Debabrata, Bimetallic PtAu alloy nanoparticles-integrated g-C_3N_4 hybrid as an efficient photocatalyst for water-to-hydrogen conversion, ACS Appl. Mater. Interfaces 11 (2019) 478–488.

[81] L. Jing, R. Zhu, D.L. Phillips, J.C. Yu, Effective prevention of charge trapping in graphitic carbon nitride with nanosized red phosphorus modification for superior photo(electro)catalysis, Adv. Funct. Mater. 27 (2017) 1703484.

[82] C. Lv, W. Li, Q. Lin, H. Yang, Y. Jiang, Y. Yu, Y. Huang, Efficient photocatalytic hydrogen evolution: a novel multi-modified carbon nitride based on physical adsorption, J. Mater. Chem. A 11 (2023) 20701–20711.

[83] L. Luo, J. Ma, H. Zhu, J. Tang, Embedded carbon in a carbon nitride hollow sphere for enhanced charge separation and photocatalytic water splitting, Nanoscale 12 (2020) 7339–7346.

[84] Y. Jiao, L. Tian, P. García-Aznar, G. Sastre, Y. Li, J. Wang, Z. He, Z. Li, H. García, Enhancement of intramolecular charge transfer in carbon nitride by attaching 2,4,5-Trichlorophenoxyacetic acid as electron acceptor units, Chem. Eng. J. 473 (2023) 145248.

[85] C. Cheng, S. Zong, J. Shi, F. Xue, Y. Zhang, X. Guan, B. Zheng, J. Deng, L. Guo, Facile preparation of nanosized MoP as cocatalyst coupled with g-C_3N_4 by surface bonding state for enhanced photocatalytic hydrogen production, Appl. Catal. B Environ. 265 (2020) 118620.

[86] Z. Huang, Y. Zhang, H. Dai, Y. Wang, C. Qin, W. Chen, Y. Zhou, S. Yuan, Highly dispersed Pd nanoparticles hybridizing with 3D hollow-sphere g-C_3N_4 to construct 0D/3D composites for efficient photocatalytic hydrogen evolution, J. Catal. 378 (2019) 331–340.

[87] H. Dong, M. Xiao, S. Yu, H. Wu, Y. Wang, J. Sun, G. Chen, C. Li, Insight into the activity and stability of rhxp nano-species supported on g-C_3N_4 for photocatalytic H_2 production, ACS Catal. 10 (2019) 458–462.

[88] Y. Li, Y. Si, B. Zhou, T. Huang, W. Huang, W. Hu, A. Pan, X. Fan, G. Huang, Interfacial charge modulation: carbon quantum dot implanted carbon nitride double-deck nanoframes for robust visible-light photocatalytic tetracycline degradation, Nanoscale 12 (2020) 3135–3145.

[89] Z. Li, D. Huang, C. Zhou, W. Xue, L. Lei, R. Deng, Y. Yang, S. Chen, W. Wang, Z. Wang, Metal-free carbon nitride with boosting photo-redox ability realized by the controlled carbon dopants, Chem. Eng. J. 382 (2020) 122657.

[90] W. Xing, C. Li, Y. Wang, Z. Han, Y. Hu, D. Chen, Q. Meng, G. Chen, A novel 2D/2D carbonized poly-(furfural alcohol)/g-C_3N_4 nanocomposites with enhanced charge carrier separation for photocatalytic H_2 evolution, Carbon 115 (2017) 486–492.

[91] X. Tian, Y. Sun, J. He, X. Wang, J. Zhao, S. Qiao, F. Li, Surface P atom grafting of g-C_3N_4 for improved local spatial charge separation and enhanced photocatalytic H_2 production, J. Mater. Chem. A 7 (2019) 7628–7635.

[92] H. Gao, Y. Guo, Z. Yu, M. Zhao, Y. Hou, Z. Zhu, S. Yan, Q. Liu, Z. Zou, Incorporating p-phenylene as an electron-donating group into graphitic carbon nitride for efficient charge separation, ChemSusChem 12 (2019) 4285–4292.

[93] Y. Zhang, S. Tang, W. Zhang, Y. Yu, Noble metal-free photocatalysts consisting of graphitic carbon nitride, nickel complex, and nickel oxide nanoparticles for efficient hydrogen generation, ACS Appl. Mater. Interfaces 11 (2019) 14986–14996.

[94] X. Zhang, K. Hu, X. Zhang, W. Ali, Z. Li, Y. Qu, H. Wang, Q. Zhang, L. Jing, Surface co-modification with highly-dispersed Mn & Cu oxides of g-C_3N_4 nanosheets for efficiently photocatalytic reduction of CO_2 to CO and CH_4, Appl. Surf. Sci. 492 (2019) 125–134.

[95] Y. Wang, L. Guo, Y. Zeng, H. Guo, S. Wan, M. Ou, S. Zhang, Q. Zhong, Amino-assisted NH_2-UiO-66 anchored on porous g-C_3N_4 for enhanced visible-light-driven CO_2 reduction, ACS Appl. Mater. Interfaces 11 (2019) 30673–30681.

[96] K. Wang, Y. Li, J. Li, G. Zhang, Boosting interfacial charge separation of $Ba_5Nb_4O_{15}$/g-C_3N_4 photocatalysts by 2D/2D nanojunction towards efficient visible-light driven H_2 generation, Appl. Catal. B Environ. 263 (2020) 117730.

[97] W. Wang, X. Zhao, Y. Cao, Z. Yan, R. Zhu, Y. Tao, X. Chen, D. Zhang, G. Li, D.L. Phillips, Copper phosphide-enhanced lower charge trapping occurrence in graphitic-C_3N_4 for efficient noble-metal-free photocatalytic H_2 evolution, ACS Appl. Mater. Interfaces 11 (2019) 16527–16537.

[98] L. Su, Q. Huang, Q. Lou, Z. Liu, J. Sun, Z. Zhang, S. Qin, X. Li, J. Zang, L. Dong, C. Shan, Effective light scattering and charge separation in nanodiamond@g-C_3N_4 for enhanced visible-light hydrogen evolution, Carbon 139 (2018) 164–171.

[99] Y. Zou, J.-W. Shi, D. Ma, Z. Fan, C. He, L. Cheng, D. Sun, J. Li, Z. Wang, C. Niu, Efficient spatial charge separation and transfer in ultrathin g-C_3N_4 nanosheets modified with Cu_2MoS_4 as a noble metal-free co-catalyst for superior visible light-driven photocatalytic water splitting, Catal. Sci. Technol. 8 (2018) 3883–3893.

[100] K. Li, Z. Huang, X. Zeng, B. Huang, S. Gao, J. Lu, Face-to-face interfacial assembly of ultrathin g-C_3N_4 and anatase TiO_2 nanosheets for enhanced solar photocatalytic activity, ACS Appl. Mater. Interfaces 9 (2017) 28674–28684.

[101] S. Tonda, S. Kumar, M. Bhardwaj, P. Yadav, S. Ogale, g-C_3N_4/NiAl-LDH 2D/2D hybrid heterojunction for high-performance photocatalytic reduction of CO_2 into renewable fuels, ACS Appl. Mater. Interfaces 10 (2018) 2667–2678.

[102] O. Elbanna, M. Fujitsuka, T. Majima, g-C_3N_4/TiO_2 mesocrystals composite for H_2 evolution under visible-light irradiation and its charge carrier dynamics, ACS Appl. Mater. Interfaces 9 (2017) 34844–34854.

[103] M. Kombo, L. Ma, Y. Liu, X. Fang, N. Ullah, A.H. Odda, A. Xu, Graphitic carbon nitride/CoTPP type-II heterostructures with significantly enhanced photocatalytic hydrogen evolution, Catal. Sci. Technol. 9 (2019) 2196–2202.

[104] X. Shi, M. Fujitsuka, Z. Lou, P. Zhang, T. Majima, In situ nitrogen-doped hollow-TiO_2/g-C_3N_4 composite photocatalysts with efficient charge separation boosting water reduction under visible light, J. Mater. Chem. A 5 (2017) 9671–9681.

[105] H. Shi, S. Long, S. Hu, J. Hou, W. Ni, C. Song, K. Li, G.G. Gurzadyan, X. Guo, Interfacial charge transfer in OD/2D defect-rich heterostructures for efficient solar-driven CO_2 reduction, Appl. Catal. B Environ. 245 (2019) 760–769.

[106] H. Huang, Z. Zhang, S. Guo, K. Cheng, J. Xu, N. Zhang, Interfacial charge-transfer transitions enhanced photocatalytic activity of TCNAQ/g-C_3N_4 organic hybrid material, Mater. Lett. 255 (2019) 126546.

[107] Z. Qin, F. Xue, Y. Chen, S. Shen, L. Guo, Spatial charge separation of one-dimensional Ni_2P-$Cd_{0.9}Zn_{0.1}S$/g-C_3N_4 heterostructure for high-quantum-yield photocatalytic hydrogen production, Appl. Catal. B Environ. 217 (2017) 551–559.

[108] N. Kumaresan, M.M.A. Sinthiya, M. Sarathbavan, K. Ramamurthi, K. Sethuraman, R.R. Babu, Synergetic effect of g-C_3N_4/ZnO binary nanocomposites heterojunction on improving charge carrier separation through 2D/1D nanostructures for effective photocatalytic activity under the sunlight irradiation, Separ. Purif. Technol. 244 (2020) 116356.

[109] K. Li, Z. Huang, X. Zeng, B. Huang, S. Gao, J. Lu, Synergetic effect of Ti^{3+} and oxygen doping on enhancing photoelectrochemical and photocatalytic properties of TiO_2/g-C_3N_4 heterojunctions, ACS Appl. Mater. Interfaces 9 (2017) 11577–11586.

[110] X. Kong, J. Fan, B. Feng, J. Li, G. Yang, C. Xue, Carbon dots-triggered the fabrication of miniature g-C_3N_4/CDs/WO_3 S-scheme heterojunction for efficient CO_2 photoreduction, Chem. Eng. J. 476 (2023) 146774.

[111] W.-K. Jo, S. Kumar, S. Eslava, S. Tonda, Construction of Bi_2WO_6/RGO/g-C_3N_4 2D/2D/2D hybrid Z-scheme heterojunctions with large interfacial contact area for efficient charge separation and high-performance photoreduction of CO_2 and H_2O into solar fuels, Appl. Catal. B Environ. 239 (2018) 586–598.

[112] P. Xia, S. Cao, B. Zhu, M. Liu, M. Shi, J. Yu, Y. Zhang, Designing a 0D/2D S-scheme heterojunction over polymeric carbon nitride for visible-light photocatalytic inactivation of bacteria, Angew. Chem. Int. Ed. 59 (2020) 5218–5225.

[113] W. Chen, Z. He, G. Huang, C. Wu, W. Chen, X. Liu, Direct Z-scheme 2D/2D $MnIn_2S_4$/g-C_3N_4 architectures with highly efficient photocatalytic activities towards treatment of pharmaceutical wastewater and hydrogen evolution, Chem. Eng. J. 359 (2019) 244–253.

[114] R. Cao, H. Yang, S. Zhang, X. Xu, Engineering of Z-scheme 2D/3D architectures with $Ni(OH)_2$ on 3D porous g-C_3N_4 for efficiently photocatalytic H_2 evolution, Appl. Catal. B Environ. 258 (2019) 117997.

[115] Z. Zhu, P. Huo, Z. Lu, Y. Yan, Z. Liu, W. Shi, C. Li, H. Dong, Fabrication of magnetically recoverable photocatalysts using g-C_3N_4 for effective separation of charge carriers through like-Z-scheme mechanism with Fe_3O_4 mediator, Chem. Eng. J. 331 (2018) 615–625.

[116] S.X. Hua, D. Qu, L. An, W.S. Jiang, Y.J. Wen, X.Y. Wang, Z.C. Sun, Highly efficient p-type Cu3P/n-type g-C3N4 photocatalyst through Z-scheme charge transfer route, Appl. Catal. B Environ. 240 (2019) 253–261.

[117] H. Xu, X. She, T. Fei, Y. Song, D. Liu, H. Li, X. Yang, J. Yang, H. Li, L. Song, P.M. Ajayan, J. Wu, Metal-oxide-mediated subtractive manufacturing of two-dimensional carbon nitride for high-efficiency and high yield photocatalytic H_2 evolution, ACS Nano 13 (2019) 11294–11302.

[118] J. Wang, Y. Xia, H. Zhao, G. Wang, L. Xiang, J. Xu, S. Komarneni, Oxygen defects-mediated Z-scheme charge separation in g-C_3N_4/ZnO photocatalysts for enhanced visible-light degradation of 4-chlorophenol and hydrogen evolution, Appl. Catal. B Environ. 206 (2017) 406–416.

[119] Y. Wu, H. Wang, Y. Sun, T. Xiao, W. Tu, X. Yuan, G. Zeng, S. Li, J. Chew, Photogenerated charge transfer via interfacial internal electric field for significantly improved photocatalysis in direct Z-scheme oxygen-doped carbon nitrogen/CoAl-layered double hydroxide heterojunction, Appl. Catal. B Environ. 227 (2018) 530–540.

[120] X. Zhang, K. Matras-Postolek, P. Yang, S.P. Jiang, Pt clusters in carbon network to enhance photocatalytic CO_2 and benzene conversion of WO_x/g-C_3N_4 nanosheets, Carbon 214 (2023) 118337.

[121] A. Pandey, U. Alam, A. Gupta, J.-J. Shim, N. Verma, S-scheme heterojunction-mediated hydrogen production over the graphitic carbon nitride-anchored nickel stannate perovskite, Fuel 355 (2023) 129538.

[122] M. Wang, S. Huang, X. Pang, M. Song, C. Du, Y. Su, Switching charge kinetics from type-I to Z-scheme for g-C_3N_4 and $ZnIn_2S_4$ by defective engineering for efficient and durable hydrogen evolution, Sustain. Energy Fuels 3 (2019) 3422–3429.

[123] X. Yu, Z. Li, J. Liu, P. Hu, Ta-O-C chemical bond enhancing charge separation between Ta^{4+} doped Ta_2O_5 quantum dots and cotton-like g-C_3N_4, Appl. Catal. B Environ. 205 (2017) 271–280.
[124] Y. Sun, K. Lai, W. Bai, N. Li, Y. Gao, L. Ge, Ultrathin Cu_2MoS_4/g-C_3N_4 nanosheets for promoting charge separation with strong redox ability and enhanced photocatalytic hydrogen production activity, Colloids Surf. A Physicochem. Eng. Asp. 684 (2024) 133156.
[125] C. Liang, C. Niu, H. Guo, D. Huang, X. Wen, S. Yang, G. Zeng, Combination of efficient charge separation with the assistance of novel dual Z-scheme system: self-assembly photocatalyst Ag@AgI/BiOI modified oxygen-doped carbon nitride nanosheet with enhanced photocatalytic performance, Catal. Sci. Technol. 8 (2018) 1161–1175.
[126] J. Zheng, L. Zhang, Designing 3D magnetic peony flower-like cobalt oxides/g-C_3N_4 dual Z-scheme photocatalyst for remarkably enhanced sunlight driven photocatalytic redox activity, Chem. Eng. J. 369 (2019) 947–956.
[127] Y. Cui, L.-c. Nengzi, J. Gou, Y. Huang, B. Li, X. Cheng, Fabrication of dual Z-scheme MIL-53(Fe)/alpha-Bi_2O_3/g-C_3N_4 ternary composite with enhanced visible light photocatalytic performance, Separ. Purif. Technol. 232 (2020) 115959.